

# Internal oxidation and oxide scales formation of Fe-33Ni-19Cr alloy

Noraziana Parimin<sup>1,\*</sup>, Esah Hamzah<sup>2</sup>

<sup>1)</sup> School of Materials Engineering, Universiti Malaysia Perlis, 02600 Arau, Perlis, Malaysia

<sup>2)</sup> Faculty of Mechanical Engineering, Universiti Teknologi Malaysia, 81310 Skudai, Johor, Malaysia

\*Corresponding e-mail: noraziana@unimap.edu.my

**Keywords:** Internal oxidation; oxide scale growth; Fe-33Ni-19Cr alloy

**ABSTRACT** – The internal oxidation and oxide scales formation of solution-treated Fe-33Ni-19Cr alloy was investigated. The internal oxidation and oxide scales was initiated by exposure of Fe-33Ni-19Cr alloy to 900°C for 500 hours in laboratory air. The oxide scales formation and cross-sectional analysis during discontinuous isothermal oxidation was examined using XRD and SEM-EDX techniques. Coarse-grained of solution-treated Fe-33Ni-19Cr alloy exhibited the thicker internal oxidation along grain boundary area compared to fine-grained sample, which are 56.0µm and 24.5µm, respectively. The formation of oxide scales was complex, composed of Cr<sub>2</sub>O<sub>3</sub>, Cr<sub>1.3</sub>Fe<sub>0.7</sub>O<sub>3</sub>, (Cr<sub>0.88</sub>Ti<sub>0.12</sub>)<sub>2</sub>O<sub>3</sub>, Fe<sub>2</sub>O<sub>3</sub>, Fe<sub>3</sub>O<sub>4</sub>, MnCr<sub>2</sub>O<sub>4</sub>, MnFe<sub>2</sub>O<sub>4</sub>, FeCr<sub>2</sub>O<sub>4</sub>, NiCr<sub>2</sub>O<sub>4</sub>, NiFe<sub>2</sub>O<sub>4</sub>, TiO<sub>2</sub> and (Ti<sub>0.97</sub>Cr<sub>0.03</sub>)O<sub>2</sub>.

## 1. INTRODUCTION

Fe-33Ni-19Cr alloy is heat-resistant alloy which developed a protective oxide scales at high temperature applications. Alloying elements that can form strengthening phases are commonly added to enhanced excellent mechanical, physical properties and oxidation resistance [1-2]. Internal oxidation is a common phenomenon observed in metal alloys at high temperatures, usually greater than 600°C [1,3]. The formation of internal oxidation tends to penetrated along the grain boundary area underneath the oxide-metal interface. Selected alloying element such as Al and Si enhanced the formation of the Al<sub>2</sub>O<sub>3</sub> and SiO<sub>2</sub> oxide beneath the oxide layer, penetrating based metal as internal oxide precipitates, which both oxides contributed to the protective consequence at experienced temperature condition [4-5]. During high temperature exposure of Fe-33Ni-19Cr alloy, the alloy is closely dependable to their oxide scales formation which contributed to further protective conditions at high temperature. Therefore, special attention was paid in this study to the stability of internal oxidation and oxide scales formation to enhanced excellent protective barrier of this oxidation resistant material.

## 2. METHODOLOGY

Fe-33Ni-19Cr alloy was used in this study with the measured chemical compositions (in wt%): 32.5 Ni, 18.9 Cr, 0.08 C, 0.053 Al, 0.49 Ti, 0.32 Si, 0.56 Mn, 0.01 P, 0.08 Cu and balance Fe. A test samples of 3mm thickness with nominal dimensions of 10mm x 10mm x 3mm were cut from as-received alloy, then undergo a solution treatment process for 3 hours at three different temperatures, namely 950°C, 1050°C and 1150°C followed by water quench. These samples are denoted as

solution-treated 950°C (ST950), solution-treated 1050°C (ST1050) and solution-treated 1150°C (ST1150). The results showed that the average grain size increased with increase in solution treatment temperature, which are 54.55µm, 60.96µm and 70.37µm for ST950, ST1050 and ST1150, respectively. The isothermal oxidation tests were investigated by means of discontinuous testing at 900°C up to 500 hours in laboratory air. The phase analysis and cross-sectional examination of oxidized samples was characterized by X-ray Diffraction (XRD), Scanning Electron Microscopy (SEM) and Energy Dispersive X-Ray Spectroscopy (EDX).

## 3. RESULTS AND DISCUSSION

### 3.1 Phase analysis of oxide scale formation

Phase identification using XRD technique of Fe-33Ni-19Cr alloy after isothermal oxidation at 900°C for 500 hours were composed of four major phases, with corresponding to their crystal structure, namely, austenite, corundum, spinel and fluorite. The formation of most intense austenite peaks corresponding to the based alloy. The corundum type oxides composed of Cr<sub>2</sub>O<sub>3</sub>, Cr<sub>1.3</sub>Fe<sub>0.7</sub>O<sub>3</sub>, (Cr<sub>0.88</sub>Ti<sub>0.12</sub>)<sub>2</sub>O<sub>3</sub> and Fe<sub>2</sub>O<sub>3</sub> were observed. The spinel oxides also detected composed of MnCr<sub>2</sub>O<sub>4</sub>, MnFe<sub>2</sub>O<sub>4</sub>, FeCr<sub>2</sub>O<sub>4</sub>, NiCr<sub>2</sub>O<sub>4</sub>, NiFe<sub>2</sub>O<sub>4</sub>, and Fe<sub>3</sub>O<sub>4</sub>. In addition, the Ti-rich oxides phases also detected composed of TiO<sub>2</sub> and (Ti<sub>0.97</sub>Cr<sub>0.03</sub>)O<sub>2</sub> oxide with fluorite crystal structure. The formation of Cr-Ti rich oxide was aforementioned to mitigate the Cr evaporation effect due to the lower Cr vapor pressure of (Cr,Ti)<sub>2</sub>O<sub>3</sub> compared to Cr<sub>2</sub>O<sub>3</sub>. Furthermore, the addition of Mn alloying element to the Fe-Ni-Cr system will give beneficial effect to the oxide scale formation due to the formation of outer Cr/Mn-spinel layer, which is known to reduce the development of volatile Cr-species [5]. Moreover, the formation of Cr/Mn-spinel layer consists of MnCr<sub>2</sub>O<sub>4</sub> reflect the rapid diffusion of Mn in Cr<sub>2</sub>O<sub>3</sub> oxide phase.

### 3.2 Cross-sectional analysis of internal oxidation

An elemental line scan SEM-EDX analysis for cross-sectional ST950 sample is shown in Figure 1. It was found that the oxide scale formed was approximately 10 µm. This sample formed a several oxide layers which are labeled as area 1, 2, 3 and 4. The cross-sectional image for ST950 sample in Figure 1 shows a formation of Cr-Mn oxide at the outer oxide layer at area 1, estimated composed of MnCr<sub>2</sub>O<sub>4</sub> and/or Cr<sub>2</sub>O<sub>3</sub> oxide phases. It was also found that thick oxides formed to cover the entire alloy surface indicate excellent protective oxide layer. This is due to the formation of Mn-Cr spinel oxides which will increase the efficiency of

protective oxide behavior because the higher solubility of Mn and Cr that will reduce the Cr volatile effect at high temperature. The Cr and Mn were depleted at area 2, indicating the enrichment of elements Fe, Ni and O. Whereas, at area 3 which is at the scale-metal interface, the enrichment of element Cr and O were recorded, indicating the formation of  $\text{Cr}_2\text{O}_3$  oxide. In addition, at point 4, indicated the enrichment of elements Al and O representing the formation of Al oxide precipitate. Similar argument made by [4-5] which stated that Al alloying addition tend to developed the Al oxide layer underneath the oxide scale, penetrating based metal as internal oxide precipitates.

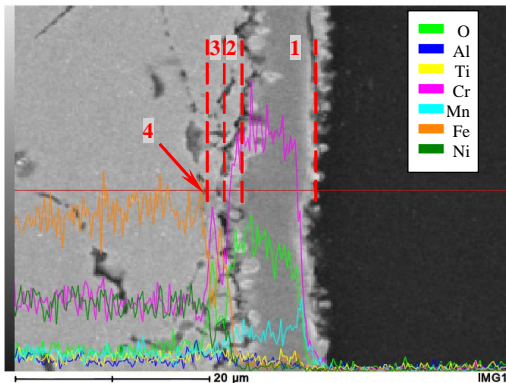


Figure 1 Cross-sectional SEM line scan image of ST950 (Magnification 2500x).

Figure 2 shows SEM image of Fe-33Ni-19Cr alloy oxidized at 900°C for 500 hours. It shows that oxidation not only occurred on the surface but internally as well. The depth of internal oxidation increases as the grain size of the alloy increases. This is due to the large grain size with relatively few grain boundaries did not form protective oxide layer but more porous structure. Thus it allows the diffusion of  $\text{O}^{2-}$  ion into the metal to form internal mixed oxides. Sample ST950 with fine grain for example has internal oxidation up to 24.5 μm. Whereas for coarse grain ST1150 sample, the internal oxidation occurred up to 56.0 μm in depth.

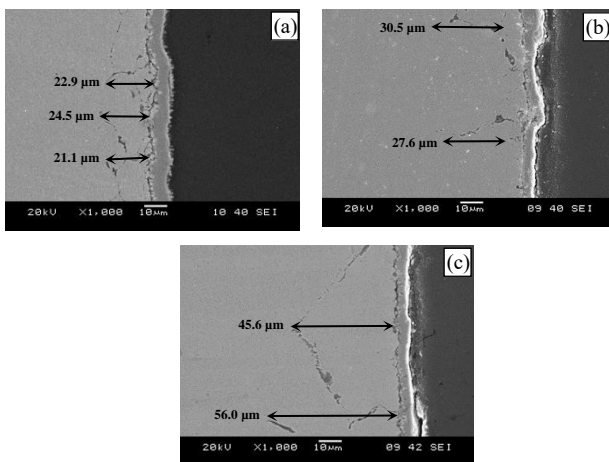


Figure 2 Cross-sectional SEM images of; (a) ST950, (b) ST1050 and (c) ST1150.

The mechanism of internal oxidation is discussed as followed. The formation of voids in the oxide scale may generated by fast metal ion diffusion along grain

boundary. Besides, oxide scale distortion and cracking due to the development of growth stress in the scale bring to the void formation. The scale above the voids generally contains a grain boundary oxide. The grain boundary area begins to open up around the void, if fast outward diffusion of metal ion along the grain boundary than through the lattice. The continuous diffusion process will open the grain boundary area as a channel of a void linkage. When open, the channel permits the oxygen ion to transmit down the channel to the metal and formed the inner oxide scale and filled the grain boundary area. The formation of internal oxide scale was restricted by the hindrance from adjacent grain which acts as a break path for further oxide penetration. The internal oxide will go deeper to the grain boundary area for the coarse grain due to the faraway location of adjacent grain to stop the penetration path. While for fine grain, the depth of the internal oxide penetration was diminishing by nearby adjacent grain, results in less internal oxide penetration. The channel will close when the void along grain boundary area filled with oxide.

#### 4. SUMMARY

The isothermal oxidation of solution-treated Fe-33Ni-19Cr alloy has been investigated at 900°C. Several oxide scales were formed on the alloy surface which increase the efficiency of protective oxide behavior. It also found that the internal oxidation was formed along the grain boundary area, which also contributed to further protection when the channel and void along grain boundary area was closed and filled with oxide scales.

#### ACKNOWLEDGEMENT

The authors would like to thank the Ministry of Education Malaysia for the research fund under the Fundamental Research Grant Scheme (FRGS) (Project Code. FRGS/1/2016/TK05/UNIMAP/02/4).

#### REFERENCES

- [1] Pan, T. J., Li, Y. S., Yang, Q., Feng, R. F., & Hirose, A. (2011). Internal oxidation and phase transformations of multi-phase Fe-Ni-Al and Fe-Ni-Al-Cr alloys induced by KCl corrosion. *Corrosion Science*, 53, 2115-2121.
- [2] Xu, Y. X., Lu, J. T., Yang, X. W., Yan, J. B., & Li, W. Y. (2017). Effect and role of alloyed Nb on the air oxidation behavior of Ni-Cr-Fe alloys at 1000°C. *Corrosion Science*, 127, 10-20.
- [3] Langelier, B., Persaud, S. Y., Newman, R. C., & Botton, G. A. (2016). An atom probe tomography study of internal oxidation processes in Alloy 600. *Acta Materialia*, 109, 55-68.
- [4] Cao, G., Firouzdor, V., Sridharan, K., Anderson, M. & Allen, T. R. (2012). Corrosion of austenitic alloys in high temperature supercritical carbon dioxide. *Corrosion Science*, 60, 246-255.
- [5] Zurek, J., Young, D. J., Essuman, E., Hansel, M., Penkalla, H. J., Niewolak, L., & Quadackers, W. J. (2008). Growth and adherence of chromia based surface scales on Ni-Base alloys in high- and low- $\text{pO}_2$  gases. *Materials Science and Engineering A*, 477, 259-270.

# Effect of semi-solid forming temperature and heat treatment on mechanical properties of Mg-Al-Zn Alloy (AZ91D) for automotive application

M.R.M. Kamal<sup>1,2\*</sup>, N.F. Bazilah<sup>1</sup>, A. Luhath<sup>1</sup>, M.H. Idris<sup>2</sup>, M.S. Salleh<sup>3</sup>, W.F.F.W. Ali<sup>2</sup>

<sup>1</sup>Fakulti Teknologi Kejuruteraan Mekanikal dan Pembuatan, Universiti Teknikal Malaysia Melaka, Hang Tuah Jaya, 76100 Durian Tunggal, Melaka, Malaysia

<sup>2</sup>School of Mechanical Engineering, Faculty of Engineering, Universiti Teknologi Malaysia, 81310 Skudai, Johor, Malaysia

<sup>3</sup>Fakulti Kejuruteraan Pembuatan, Universiti Teknikal Malaysia Melaka, Hang Tuah Jaya, 76100 Durian Tunggal, Melaka, Malaysia

\*Email: mohamadridzuan@utem.edu.my

**Keywords:** Ultimate tensile test; hardness; heat treatment

**ABSTRACT** – Magnesium alloy usage in manufacturing engineering components resulting in weight reduction and as a consequence, reduction in fuel and energy consumption. Magnesium has a relatively low density and roughly 30% lower than aluminum. However, magnesium is considered to be difficult to deform because of the HCP structure. In this present work, the effect of semi-solid forming temperature and heat treatment on mechanical properties of Mg-Al-Zn were investigated. Mg-Al-Zn ingot was machined into a billet and formed with three different temperatures and underwent T4 heat treatment process. To determine the mechanical properties of the magnesium alloy, tensile and hardness test were performed and the result indicates that the highest average maximum tensile stress was achieved at 209 MPa at 530°C after forming with T4 heat treatment and highest hardness value was at 21.44 HRB at 560°C. The heat treatment of T4 had proved its capability to alter the microstructure and gave out the higher hardening quality.

x 100mm as in Figure 1(a). T4 heat treatment involves 20 hours of process time at 415°C. The sample label A1 and A2 is a reference billet and T4 heat treated respectively. Sample B1, B2, and B3 has undergone a forming temperature of 510°C, 530°C and 560°C by induction heating as in figure 1b) and figure 1c) show the as-form billet. K type thermocouple was used to determine the forming temperature. The summary of the experimental parameter as in Table 1.

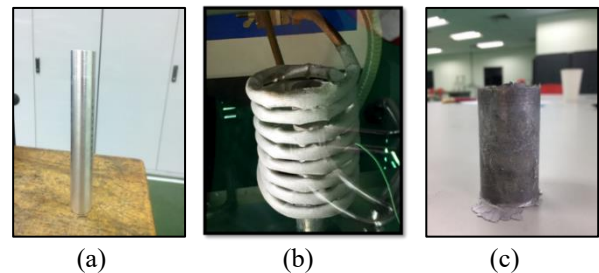


Figure 1 (a) Billet, (b) induction heating and (c) as-form billet.

## 1. INTRODUCTION

Mg is one of the most widely distributed elements in nature, ranks eighth, accounting for about 2.25% of the mass of the earth's crust. Mg, however, has poor workability at room temperature owing to its crystal structure [1]. In the past few years, the usage of Mg in the automobile industry is significantly increased. Although the automobile industry will keep on to be the foremost driving force for the future growth in magnesium applications, other areas, such as aerospace, electronics, and health care, will take a sizeable share of the magnesium market in the near future. Further growth in magnesium applications will basically depend on the successful development of new processing technologies that capable of fabricating high quality and low-cost components with higher operating temperatures.

## 2. METHODOLOGY

An ingot AZ91D magnesium alloy was used as experimental material in this work. AZ91D contains 9% of aluminum and 1% zinc and the balance is magnesium, which is a commercial use for the die casting process. Ingot was cut and machined into a billet dimension Ø20

Table 1 Experimental process parameter.

Samples	Process parameter	Forming temperature
A1	Reference Billet	-
A2	T4 HT	-
B1	Induction heating + Forming	510°C
B2	Induction heating + Forming	530°C
B3	Induction heating + Forming	560°C
C1	Induction heating + Forming + T4 HT	510°C
C2	Induction heating + Forming + T4 HT	530°C
C3	Induction heating + Forming + T4 HT	560°C

After all the samples were formed and undergo the heat treatment processes, samples were cut into a tensile test dimension by wire electrical discharge machining according to ASTM 557M-10 with a thickness of 6mm. For the Rockwell hardness test, the 100kgf load with indenter of 1/16 inch steel ball was used.

### 3. RESULTS AND DISCUSSION

Figure 2 shows a comparison of Ultimate Tensile Strength (UTS) of all samples. The UTS for as-cast (A1) is 219 MPa, as-cast + T4 heat treatment (A2) is 255 MPa. Forming at 510°C (B1) is 157 MPa, forming at 530°C (B2) is 161 MPa, forming at 510°C (B3) is 150 MPa, forming at 510°C + T4 heat treatment (C1) is 182 MPa, forming at 530°C + T4 heat treatment (C2) is 209 MPa, and lastly forming at 560°C + T4 heat treatment (C3) is 174 MPa. The graph from figure 2 showed forming at 560°C (B3) obtained the lowest UTS when compared to the all average of the samples and highly differences from expected. Although the highest UTS receive from the sample as-cast + T4 heat treatment (A2), the samples are not yet formed compare with the sample forming at 530°C + T4 heat treatment (C2). In the term of finish goods, samples that are already formed is more reliable compared to as-cast. The UTS trend from sample B1, B2, B3, C1, C2, and C3 was slightly increased at the forming temperature of 530°C and decrease at the temperature 560°C. It shows that the sensitivity to temperature gives a significant effect on the strength of the forming material. Meanwhile, at the as-cast stage, the strength of AZ91D is high compared to the at the forming stage. The forming sample in this study showed an inconsistent result where it's value does not exceed the as-cast UTS result. In the previous study on the effect of forming on A390 aluminum's mechanical properties, the UTS can reach as high as 293MPa, this kind of result was to expected when tested on AZ91D forming sample.

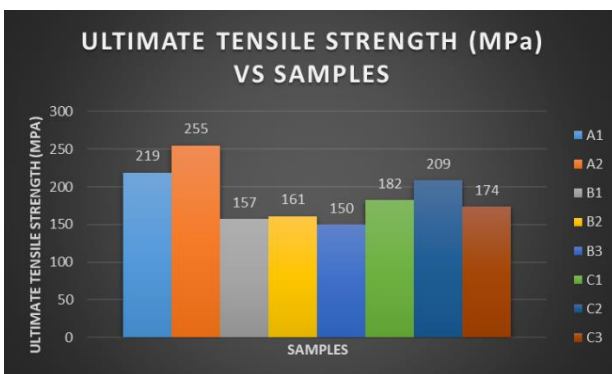


Figure 2 Ultimate tensile strength vs. samples.

Figure 3 shows a comparison of the hardness test (HRB) of all samples. The hardness test for as-cast (A1) is 13.41 HRB, as-cast + T4 heat treatment (A2) is 13.26HRB. Forming at 510°C (B1) is 17.63HRB, forming at 530°C (B2) is 17.52HRB, forming at 510°C (B3) is 21.44HRB, forming at 510°C + T4 heat treatment (C1) is 16.77HRB, forming at 530°C + T4 heat treatment (C2) is 17.52HRB, and lastly forming at 560°C + T4 heat treatment (C3) is 21.07HRB. The graph from figure 3 showed as-cast +T4 (A2) obtained the lowest hardness value when compared to all average of the samples. The

highest hardness value is forming at 560°C and forming at 560°C+T4 heat treatment where 21.44 HRB and 21.07HRB respectively. It shows that forming temperature at 560 °C gives a significant effect on the hardness of AZ91D material but gives among the lowest ultimate tensile strength value.

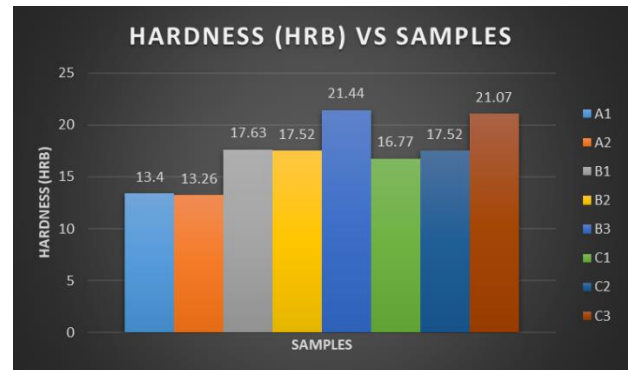


Figure 3 Hardness vs. samples.

### 4. CONCLUSION

The mechanical properties covered in this study was tested using a tensile test where the ultimate tensile strength (UTS) was observed. The result of the tensile test showed that the T4 gave out the highest UTS for the as-cast sample. Meanwhile, it varies when it comes to semisolid forming sample. In the result of the hardness value in the Rockwell test showed that forming with 560°C gave out the highest value. Meanwhile, the hardness value of the forming at 560°C + T4 sample gives the second highest. T4 heat treatment and without heat treatment were both comparable, with T4 showed a slightly lower value. This could be the result of lack in precipitate by T4 treatment or probably due to the indent might partially land on the  $\alpha$ -mg region or eutectic mixture causing a variety of the result.

### ACKNOWLEDGMENT

The authors gratefully acknowledged the financial support from Universiti Teknikal Malaysia Melaka and The Ministry of Education, Malaysia under Research Grant number. PJP/2018/FTK(2C)/S01586.

### REFERENCES

- [1] Yan, J., Xie, J., Yuan, J. S., Zhang, J. Y., & Guo, T. (2014). The influence of alloy elements on Mg-Al alloy and its development Prospect. *Applied Mechanics and Materials*, 687, 4283-4286.
- [2] Furui, M., Sakashita, S., Suzuki, S., Aida, T., Ishisaka, Y., Yamamoto, M., & Ohta, M. (2017). Aging property of AZ91D magnesium alloy screw thread-rolled at room temperature using extrusion-torsion simultaneous processing. *Materials Science Forum*, 879, 2450-2455.



# Fabricate flow channel of bipolar plate through milling machining process

Mohd Zulkefli.Selamat<sup>1,2,\*</sup>, HamzaitulAkmarizal Hamdan<sup>1,2</sup>, Mohd Basri Ali<sup>1,2</sup>, Sivakumar Dhar Malingam<sup>1,2</sup>

<sup>1)</sup> Fakulti Kejuruteraan Mekanikal, Universiti Teknikal Malaysia Melaka, Hang Tuah Jaya, 76100 Durian Tunggal, Melaka, Malaysia

<sup>2)</sup> Centre for Advanced Research on Energy, Universiti Teknikal Malaysia Melaka, Hang Tuah Jaya, 76100 Durian Tunggal, Melaka, Malaysia

\*Corresponding e-mail: zulkeflis@utem.edu.my

**Keywords:** PEMFC bipolar plate; serpentine; interdigitated

**ABSTRACT** – This research objective is investigating the accuracy of producing flow channel on a bipolar plate by the machining process. The bipolar plates used are G/CB/Fe/PP composites, V shape of the serpentine and U shape of the interdigitated flow channel has been selected. The flow channel fabricated by machining used flat End Mill with a diameter of 1.5 mm as cutting tool to fabricate the flow channel. The specimen dimensions of width, channel width 1, channel width 2 and channel depth have been measured and compare to actual drawing. Serpentine (V shape) and interdigitated (U shape) specimens with 2 mm width delivers better dimension accuracy with less of the 4.13% margin of error. Except the channel depth with the maximum margin of error is 30.2 % for U shape, but for serpentine (V shape) the channel depth with the maximum margin of error is 18 % which is better than U shape.

## 1. INTRODUCTION

Polymer Electrolyte Membrane Fuel Cell or Proton Exchange Membrane Fuel Cell (PEMFC) has been identified as a power source for many applications and the development of this sector rapidly expanding from year to year. It is because of PEMFC promising many advantages compared to other fuel cells, such as low temperature operation, quick startup time and dynamic operation capabilities [1]. PEMFC has huge potential to be commercialized because of high energy conversion efficiency and low pollutant emission [2].

In commercialize of PEMFC high cost and durability of PEMFC become a barrier to widespread the commercialization [3]. Bipolar plate were categories by it flow channel design. The most popular flow channel designs are serpentine and interdigitated flow channel as shown in Figure 1. The serpentine flow channel was popular as their pressure drop requirements and water removal rate correlates each other [4]. Interdigitated flow channel consists of multiple dead-ended flow channels and it forced gas flow through the adjacent diffusion layer.

Graphite has become major bipolar plate materials due to adequate electrical conductivity, light weight and good corrosion resistance but producing precise flow field channels is difficult and expensive due to brittleness issue [5]. Conducting Polymer Composite (CPC) offers better mechanical properties to wind stand the stress force during the machining process. This research aim is to investigate the fabrication of flow

channel through the machining process of specimen dimensions (width, channel width 1, channel width 2 and channel depth) of flow channel will be measured and compare with actual drawing.

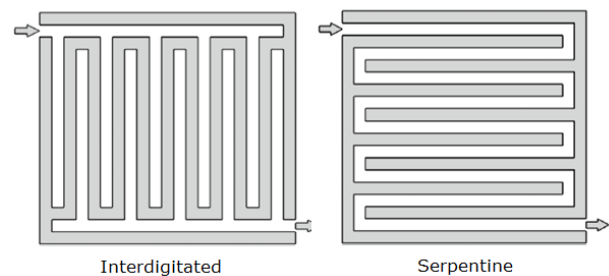


Figure 1 Interdigitated and serpentine flow channel.

## 2. METHODOLOGY

### 2.1 Fabrication of Polymer Composites

All fillers were mixed by using ball mill machine for 1½ hours. After that, G/CB/Fe/PP were further mixed using Haake Poly lab Rheodrive Internal Mixer machine at the temperature of 200° C, rotor speed of 50 RPM and duration time of 15 minutes. After that the mixture was collected and has been pulverized to further refine using Retsch ZM200 Pulverizer. Compression molding method has been chosen to shape the sample and Gotech (GT 7014 – A) hot press machine was used. The temperature has been set at 185°C, preheating times is about 10 minutes and pressure was set at 50 tons and the duration of pressing time is about 10 minutes. After that the mold has been cooled down about 15 minutes before specimen relished from mould.

### 2.2 Flow Channel Drawing Process

Flow channel was drawn by a CAD program. Main parameters have been selected as show in Table 1.

Table 1 Parameters of flow field design.

Parameters of flow channel	Plate
Dimension	50 mm x 50 mm
Type of flow channel	U Interdigitated & V Serpentine
Width of flow channel	1 mm & 2 mm
Depth of flow channel	0.5 mm
Taper angle of flow channel	45°

They are three different designs were drawn,

serpentine V with 1 mm and 2 mm depth and interdigitated U shape with 2 mm depth. Figure 2 shows a CAD drawing for both flow channel design.

### 2.3 Fabrication of Flow Channel by Machining

The machining process of flow channel for U and V shapes on the surface of plate was used Bridgeport Model GX 710 with spindle speed of 4000 RPM, feed

rate of 400 mm/min and cutting tool is flat End Mills with a diameter of 1.5 mm.

### 2.4 Measurement Test

The specimens were measured to determine the dimension parameters. Smartscope CNC500 was used to measure specimen dimensions (width, channel width 1, channel width 2 and channel depth).

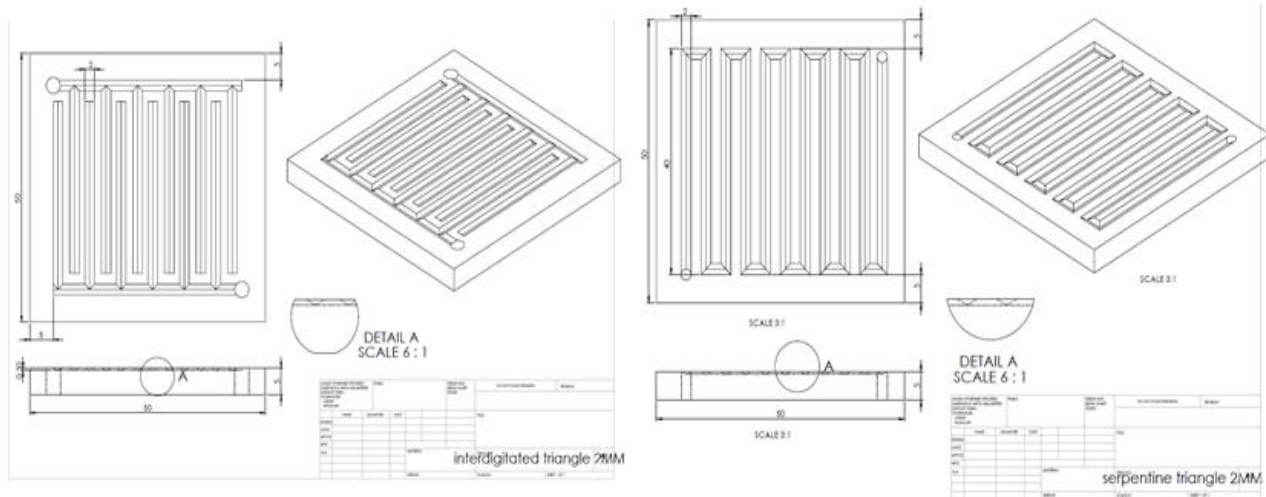


Figure 2 CAD drawing for serpentine and interdigitated.



Figure 3 Smartscope CNC500.

## 3. RESULTS AND DISCUSSION

### 3.1 Serpentine V Shape

Figure 4 shown serpentine flow channel type specimens. Both specimens are serpentine V shape with 45° draft angles with 2 mm and 1 mm channel width.

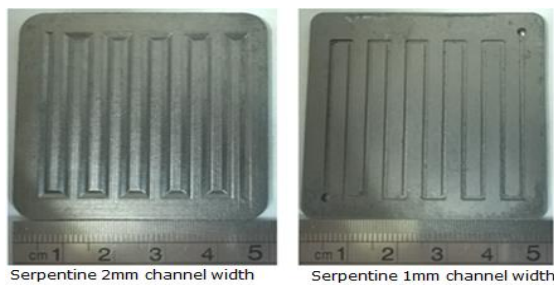


Figure 4 Serpentine V shape flow channel specimens.

### 3.2 Interdigitated U Shape

Figure 5 shown the interdigitated flow channel with 2 mm channel width.



Figure 5 Interdigitated U shape flow channel.

### 3.3 Measurement Test Result

There are 4 dimensional points which are 1 up to 4 were measured and recorded using Smartscope. While

Table 2 shows measured value of dimension versus drawing.

Table 2 Specimen measurement vs drawing.

No	Point of Dimensions	Drawings (mm)	Serpentine (V shape)						Interdigitated (U shape)		
			1 mm channel			2 mm channel					
			Spec.	Different		Spec.	Different		Spec.	Different	
				mm	%		mm	%		mm	%
1	Width	50	49.97	0.03	0.06	50.096	-0.096	0.192	49.919	0.081	0.162
2	Channel Width 1	1 or 2	1.7	-0.7	70.0	1.946	0.054	2.7	2.034	-0.034	1.7
3	Channel Width 2	1 or 2	1.374	-0.374	37.4	1.919	0.081	4.05	2.022	-0.022	1.1
4	Channel Depth	0.5	0.556	-0.056	11.2	0.591	0.091	18.2	0.651	-0.151	30.2

Table 2 shows that V shape serpentine and U shape interdigitated specimens with 2 mm channel produce by machining process have a better dimension accuracy than serpentine with 1 mm channel width. Meanwhile, Serpentine and interdigitated specimens with 2 mm width delivers better dimension accuracy with less of the 4.13% margin of error. Except the channel depth with the maximum margin of error is 30.2 % for U shape, but for serpentine (V shape) the channel depth with the maximum margin of error is 18 %.

### 4. CONCLUSION

As a conclusion, the flow channel of bipolar plate is suitable to be machined due to its good mechanical properties to withstand the stress force during the machining process. Serpentine and interdigitated specimen with 2 mm width delivers better dimension accuracy with less of the 4.13% margin of error except the channel depth.

### ACKNOWLEDGEMENT

The authors would like to thank the Malaysia Ministry of Higher Education, Malaysia and Ministry of Science, Technology and Innovation for sponsoring this work under Gant FRGS (RACE) /2013/FKM/TK2/2 F00203 and Universiti Teknikal Malaysia Melaka (UTeM) for financially sponsoring during this research.

### REFERENCES

- [1] Baker, R., Zhang, J. (2011). Proton exchange membrane or polymer electrolyte membrane (pem) fuel cells. *Electrochemistry Encyclopedia*.
- [2] Kumar, A., & Reddy, R. G. (2003). Effect of channel dimensions and shape in the flow-field distributor on the performance of polymer electrolyte membrane fuel cells. *Journal of power sources*, 113(1), 11-18.
- [3] Selamat, M. Z., Sahari, J., Muhamad, N., & Muchtar, A. (2011). Simultaneous Optimization for multiple responses on the compression moulding parameters of composite graphite-polypropylene using Taguchi method. *Key Engineering Materials*, 471, 361-366.
- [4] Yusuf, M. Y. M., Selamat, M. Z., Sahari, J., Daud, M. A. M., Tahir, M. M., & Hamdan, H. A. (2017). Fabrication of a flow channel for production of polymer composite bipolar plate through hot compression molding. *Journal of Mechanical Engineering and Sciences*, 11(1), 2428-2442.
- [5] Selamat, M. Z., Masron, F., Yusuf, M., Yusri, M., Kamarolzaman, A. A., Mohd Tahir, M., & Herawan, S. G. (2015). Effect of stannum on properties of graphite/stannum composite for bipolar plate. *Applied Mechanics and Materials*, 699, 157-162.

# Development of biodegradable plastic with natural sources as packaging material

Mohammad Khalid Wahid\*, Mohd Nazri Ahmad, Nurul Ain Maidin, Mohd Hairizal Osman, Mohd Hidayat Ab Rahman

Fakulti Teknologi Kejuruteraan Mekanikal dan Pembuatan, Universiti Teknikal Malaysia Melaka,  
Hang Tuah Jaya, 76100 Durian Tunggal, Melaka, Malaysia

\*Corresponding e-mail: mohammadkhalid@utem.edu.my

**Keywords:** Biodegradable; plastic; fiber

**ABSTRACT** – This paper presents the comparison of mechanical properties of three different biodegradable plastics made from tapioca starch that mixture with natural fiber such as oil palm fiber and sugar cane fiber. The application of this research is to produce biodegradable plastic packaging for the food industry purpose. Tapioca starch was used as the main ingredient with sugar cane fiber and oil palm fiber mixture in three different variations. Then these biodegradable plastics were evaluated with the tensile test and biodegradable test. The tensile test had shown that sugar cane fiber sample has 0.29 MPa, oil palm fiber has 1.12 MPa and mixture fiber has 0.33 MPa.

## 1. INTRODUCTION

Starch is a biodegradable, inexpensive and abundantly available polysaccharide molecule. It is widely distributed in the form of tiny granules as the reserve carbohydrate in stems, roots, grains and fruits of all forms of green leafed plants [1]. Tapioca flour was the thermoplastic material through the disruption of the molecular chains under specific conditions of temperature and presence of plasticizer. The process of compression molding was selected as the manufacturing process in which recharges containing chopped fibers were compressed in a mold. The structural fibers need to produce were volume fraction homogeneous and isotropic fiber orientation structure. This changes the fiber caused by the flow characteristics that are produced during the charging process. The mechanical properties of the final product are determined predominantly by fiber [2]. Tensile properties of composites are improved by adding fibers to the polymer matrix of the fiber strength and stiffness values were higher than the matrix [3]. Environmental properties evaluation of the natural fiber biopolymer composite were depended on the ingredient composite, filler content, fibers orientation, interfacial bonding, and the processing applied in the fabricated process. Biodegradation test was performed to evaluate performance degradation rates and environmental impacts caused by the sample. In the research, works were included biodegradation testing in weathering test and soil test. The objectives of this research are to produce biodegradable plastics with a complete investigation of the tensile strength and evaluated the biodegradation level of each sample.

## 2. METHODOLOGY

The raw material that involved in this study were are tapioca starch as a matrix material and the reinforcement which are sugar cane fiber and oil palm fiber. The glycerol was selected as the plasticizers in this composite. The liquid form of glycerol from vegetables was used in this study. Tapioca starch was selected as a matrix in the composite fabrication. Tapioca was abstract into the powder form. Tapioca starch is available in the market as a commodity tapioca starch. In this study, nature fiber was obtained from sugar cane and oil palm fiber. The cleaning process should be emphasized to ensure that the fiber is not contaminated with foreign bodies. The nature fiber was crushed into the blender to get the specific length and size. The drying process should be repeated to ensure that the fiber density is constant and make sure no moisture entrapped between the sugar cane and oil palm fiber. The formulation was divided into three main compositions of the weight ratio of the fiber loading. Then all the raw materials that used were weighed according to the analytical balance. In this research, the glycerol content is fixed in 5% addition as an additive in the mixture. Table 1 shows the composition of raw materials

Table 1 Sample composition.

Sample	Fiber	Tapioca	Glycerol
Sugar Cane Fiber	60 %	35%	5%
Oil Palm Fiber	60%	35%	5%
Mixture Fiber	30%+ 30%	35%	5%

After the fabrication of these composites was made by compression molding process, the samples were prepared for tensile test (ASTM D638-10) and biodegradable test or soil test (ASTM-6400-99). Each sample was labeled for each container. The time and date were recorded on the sample material placed in the ground. This biodegradable test was regularly checked to monitor the status of degradation since has been planted. Eventually, final inspection in two weeks after planted the specimens.



### 3. RESULTS AND DISCUSSION

The results had established and observed in Figure 1, Figure 2 and Figure 3. From the product point of view, the product from oil palm fiber was darker as compared to the product of sugarcane which was brighter in terms of color display. This was due to the original color of the base material which did not change during the process. Meanwhile, the product of a mixture of oil palm and sugar cane fiber look was in intermediate color brightness. These color difference of the composite significantly important because showed physical appearance for the finished product.



Figure 1 Biodegradable plastic of oil palm fiber.



Figure 2 Biodegradable plastic of sugar cane fiber.



Figure 3 Biodegradable plastic of mixture fiber.

The average tensile test results and modulus young were shown in Table 2. These were averaging of five samples tested. The average ultimate tensile stress of palm fiber samples had shown highest value of 1.12 MPa as compared to sugar cane fibers that shown the lowest result of 0.29 MPa. Meanwhile average ultimate tensile stress of the mixture of oil palm fiber and sugar cane yield point was 0.33 MPa

Table 2 Tensile test results.

Sample	Ultimate Tensile Strength (MPa)	Modulus Young (MPa)
Sugar Cane Fiber	0.29	154.68
Oil Palm Fiber	1.12	217.67
Mixture Fiber	0.33	132.40

There are many factors that can affect the performance of natural fiber reinforced composites [4]. The difference was due to the strength of the features that were present in palm fiber were tough and compact as compared to the fiber from sugar cane. Modulus young's also known as the elastic modulus was a measurement of the material stiffness. In order to adjust the stiffness of

the material it was to normalize the load with the cross-sectional area. For biodegradable test result for each samples had shown in Figure 4, Figure 5 and Figure 6 after two week run the test.

### 4. CONCLUSION

As the conclusion of this research, the product of biodegradable plastics using starch and nature fiber were successfully prepared by mixing process, heating process, molding process, and drying process. Two standard tests were carried out to characterize the tensile strength test and the biodegradable test had shown significant result that these biodegradable plastics can performed as a packaging product and eco-friendly.

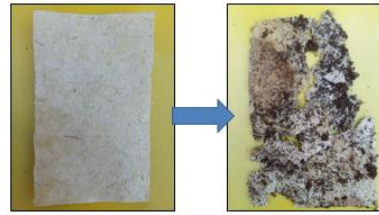


Figure 4 Sugar cane biodegradable test result.

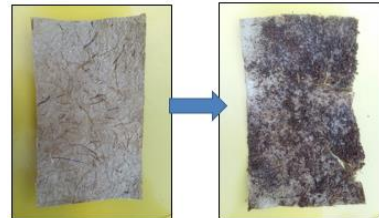


Figure 5 Oil palm biodegradable test result.

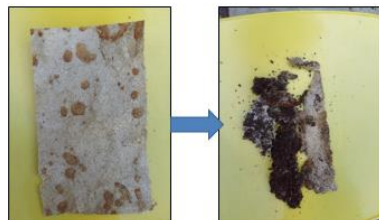


Figure 6 Mixture fiber biodegradable test result.

### REFERENCES

- [1] Neelam, K., Vijay, S., & Lalit, S. (2012). Various techniques for the modification of starch and the applications of its derivatives. *International research Journal of pharmacy*, 3(5), 25-31.
- [2] Kim, M. S., Lee, W. I., Han, W. S., & Vautrin, A. (2011). Optimisation of location and dimension of SMC precharge in compression moulding process. *Computers & Structures*, 89(15-16), 1523-1534.
- [3] Ku, H., Wang, H., Pattarachaiyakoo, N., & Trada, M. (2011). A review on the tensile properties of natural fiber reinforced polymer composites. *Composites Part B: Engineering*, 42(4), 856-873.
- [4] Ku, H., Wang, H., Pattarachaiyakoo, N., & Trada, M. (2011). A review on the tensile properties of natural fiber reinforced polymer composites. *Composites Part B: Engineering*, 42(4), 856-873.

# Preliminary study of mechanical properties for different curing period of kenaf mix with glutinous rice through tensile and impact test

Mohd Afdhal Shamsudin<sup>1,3,\*</sup>, Muhammad Hanif Mansor<sup>1</sup>, Muhammad Ilman Hakimi Chua Abdullah<sup>1,3</sup>,  
Mohd Noor Asril Saadun<sup>2,3</sup>

<sup>1</sup>) Fakulti Teknologi Kejuruteraan Mekanikal Dan Pembuatan, Universiti Teknikal Malaysia Melaka,  
Hang Tuah Jaya, 76100 Durian Tunggal, Melaka, Malaysia

<sup>2</sup>) Fakulti Kejuruteraan Mekanikal, Universiti Teknikal Malaysia Melaka,  
Hang Tuah Jaya, 76100 Durian Tunggal, Melaka, Malaysia

<sup>3</sup>) Centre for Advanced Research on Energy, Universiti Teknikal Malaysia Melaka,  
Hang Tuah Jaya, 76100 Durian Tunggal, Melaka, Malaysia

\*Corresponding e-mail: afdhal@utem.edu.my

**Keywords:** Kenaf fibre; glutinous rice; fibre

**ABSTRACT** – The purpose of this research is to analyse new composition of naturally made resin reinforced kenaf fibre on the mechanical properties of kenaf mix with natural binder. The naturally made resin used is glutinous rice that acts as a reinforcing substance for kenaf fibre. Total 24 samples were prepared by mixing the glutinous rice layer by layer with variations of kenaf in the middle. The samples were tested through tensile test and charpy impact test to identify its mechanical properties. The best composition for tensile and charpy impact test are 40% and 45% of kenaf fibre respectively.

## 1. INTRODUCTION

Kenaf or Hibiscus cannabinus is one of the herbaceous, annual, and short-photoperiod fiber which obtained from the stems of the plants in the Malvaceae family [1]. Kenaf is a type of fiber which has very light weight and porous where the bulk density of kenaf is at 0.10 until 0.20 g/cm<sup>3</sup> [2]. Furthermore, it is biodegradable and does not have site effect to the environment and human's health. Nowadays, many kenaf fiber-reinforced composite has been in used in many engineering applications or industrial sectors such as construction, automotive, marine and other mass production industries.

There is increasing in the awareness toward the environment since now the temperature of the world has increasing and the environment pollution becomes worst. Synthetic fibre causes a problem to environment and human's health. This is because the source to make is from petrochemical sources which are made up using high temperature industrial processes such as hot extrusion which produce a high amount of carbon dioxide. Temperature of the world has increased and causes the sea level increase.

Waste management system in Malaysia is very poor because the cost of dispose of the waste is increasing where the waste of produced by Malaysia is 30000 every day and only 5% of it can be recycle. More than 50% of plastic product is made up from fossil fuels [3]. After human used it, they discard to the environment by burning it since it is very hard to dispose. The burning process cause a major problem since it can produce toxic gas and it is harmful toward environment and human.

## 2. METHODOLOGY

The gel time for glutinous rice was prepared with 5 samples and dried under room temperature. The room temperatures were estimated to be 32°C. All 5 samples were calculated to obtain the average time required for the glutinous rice to cure from moist-solid state to hard and durable surface. The test procedure and mould was prepared according to ASTM D3039 for tensile testing and ASTM D6110 for impact testing. The kenaf was 100% filled inside the mould and total weight is measured as shown in Figure 1.



Figure 1 (a) Kenaf in impact mould and (b) kenaf in tensile mould.

Sample calculation in obtaining the percentage of kenaf during sample preparation as indicated below:

Mass of impact mould = 50.047g  
Mass of tensile mould = 114.360g  
Mass of impact mould + kenaf = 52.622g  
Mass of tensile mould + kenaf = 118.949g  
Mass of kenaf in impact mould = 2.575g  
Mass of kenaf in tensile mould = 4.589g

Table 1 Composition for both impact & tensile.

Composition for impact specimen	Composition for tensile specimen
$\frac{30}{100} \times 2.575g = 0.7725g$	$\frac{30}{100} \times 4.589g = 1.3767g$
$\frac{35}{100} \times 2.575g = 0.9013g$	$\frac{35}{100} \times 4.589g = 1.6062g$
$\frac{40}{100} \times 2.575g = 1.0300g$	$\frac{40}{100} \times 4.589g = 1.8356g$
$\frac{45}{100} \times 2.575g = 1.1588g$	$\frac{45}{100} \times 4.589g = 2.0651g$
$\frac{50}{100} \times 2.575g = 1.2875g$	$\frac{50}{100} \times 4.589g = 2.2945g$
$\frac{55}{100} \times 2.575g = 1.4163g$	$\frac{55}{100} \times 4.589g = 2.5240g$

Table 1 show the total weight of kenaf in one sample starting for 30wt.% up to 55wt.% for both impact and tensile specimens [4]. The glutinous rice was mix with water for about 1:1 ratio and allowed to be heated in the next process. After 15-20 minutes later, the water was filtered and reheated by using a glutinous rice cooker. Next stage is mixing slaked lime with water and added to the filtered glutinous rice. Last but not least, the complete specimen was inserted into impact and tensile mould.

The first layer of the specimen is glutinous rice, followed by kenaf and another layer of glutinous rice again to fully wrap the kenaf. There are 6 compositions related which is 30%, 35%, 40%, 45%, 50%, 55%. The mechanical properties of kenaf mix with a natural binder were conducted using tensile test and impact test based on ASTM D3039 and ASTM D6110 standard respectively.

### 3. RESULTS AND DISCUSSION

Based on Figure 2 and Figure 3, the specimen of kenaf composition 40% to 45% is the most suitable choice standard to replicate or design products made from composition of glutinous rice and kenaf due to highest value of modulus of elasticity and has the highest resistance for plastic deformation before fracture. Moreover, it can support more load compare to the rest of composition.

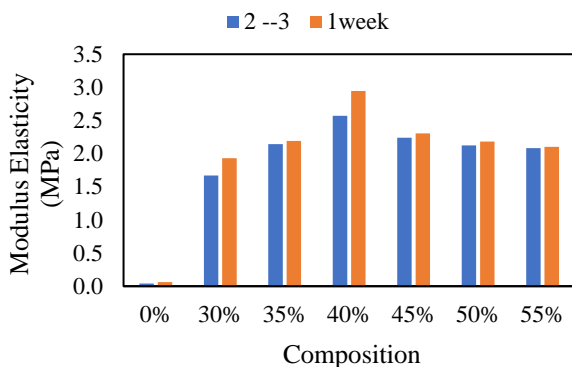


Figure 2 Modulus of elasticity for 1 week and 2-3 days curing time for each composition.

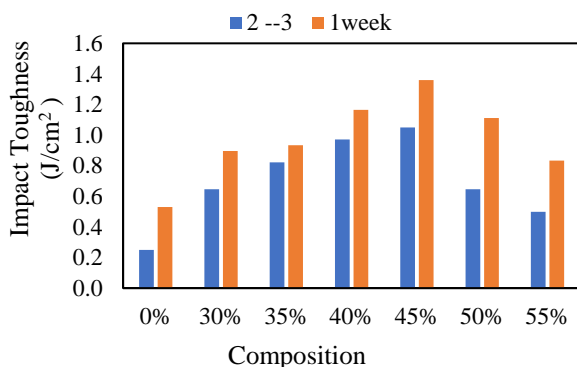


Figure 3 Impact toughness for 1 week and 2-3 days curing time for each composition.

Furthermore, it was clearly showing that 1-week cure has higher interfacial bonding compare to 2-3 days'

cure [5]. The comparison of curing time indicates that the longer the curing time, the higher the value of tensile strength, Young's Modulus and fracture strain on the specimen. Therefore, it can be concluded that the mechanical properties of kenaf fibre highly depend on the curing time where the longer the curing time, the better the interfacial bonding.

Higher degree of curing would result in higher cross-linking density which in return increases E-Modulus. Besides that, it would also decrease the strain of fracture occurred on the specimen cause Young's modulus is relatively independent of the specimen's range of composition. It is observed that the Young's modulus and automatic modulus are relatively sensitive to the change of composition [6].

### 4. CONCLUSION

As conclusion, the new composition of naturally made resin reinforced kenaf fiber was successfully made by using glutinous rice reinforced with kenaf fiber. From result, 40% and 45% composition indicate the highest value of Young's Modulus and impact toughness which is 2.945MPa and 1.36 J/cm² respectively for 1 week curing time. Further work needed to evaluate information about the surface topography and composition of the kenaf fibre.

### ACKNOWLEDGEMENT

The authors would like to thank Universiti Teknikal Malaysia Melaka (UTeM) for funded support through grant PJP/2018/FTK(2C)/S01586.

### REFERENCES

- [1] Basri, M. H. A., Abdu, A., Junejo, N., Hamid, H. A., & Ahmed, K. (2014). Journey of kenaf in Malaysia: A Review. *Scientific Research and Essays*, 9(11), 458-470.
- [2] Yahya, M. N., & Chin, D. D. V. S. (2017, August). A review on the potential of natural fibre for sound absorption application. *IOP Conference Series: Materials Science and Engineering*, 226(1), 012014.
- [3] Elsayy, M. A., Kim, K. H., Park, J. W., & Deep, A. (2017). Hydrolytic degradation of polylactic acid (PLA) and its composites. *Renewable and Sustainable Energy Reviews*, 79, 1346-1352.
- [4] Kaewpirom, S., & Worrarat, C. (2014). Preparation and properties of pineapple leaf fiber reinforced poly (lactic acid) green composites. *Fibers and Polymers*, 15(7), 1469-1477.
- [5] Samsudin, N. S., Shamsudin, M. A., & Abdullah, M. I. H. C. (2017). Effect of different composition of kenaf fiber and polyester as composite fiber substitution on elasticity profile properties. *Proceedings of Mechanical Engineering Research Day 2017*, 2017, 333-334.
- [6] Naik, D. L., & Kiran, R. (2018). On anisotropy, strain rate and size effects in vat photopolymerization based specimens. *Additive Manufacturing*, 23, 181-196.

# The effects of filler fibre sizes on the mechanical and fracture morphology of dried banana leaves filled recycled polypropylene

Thinakaran Narayanan<sup>1,2,\*</sup>, Jeefferie Abd Razak<sup>1</sup>, Intan Sharhida Othman<sup>1</sup>

<sup>1)</sup> Fakulti Kejuruteraan Pembuatan, Universiti Teknikal Malaysia Melaka, Hang Tuah Jaya, 76100, Durian Tunggal, Melaka, Malaysia

<sup>2)</sup> Department of Mechanical Polymer, National Youth High Skill Institute (IKTBN) Sepang, Bandar Baru Salak Tinggi, 43900, Sepang, Selangor, Malaysia

\*Corresponding e-mail: thinakaran@utem.edu.my / thinakaran@kbs.gov.my

**Keywords:** DBLF; filler size; mechanical

**ABSTRACT** – Natural fibre play an important role in the mechanical properties. The composite between dried banana leaves fibre (DBLF) and waste polypropylene (rPP). DBLF has been grounded into 10 $\mu$ m and 30 $\mu$ m of fibre sizes and the rPP crushed into finer particles. Composites are prepared through melting device and an injection moulding process for both fibre sizes and loading (0, 10, 20, 30 and 40) wt. %. It resulted more strength in tensile of 10 $\mu$ m rPP/DBLF composite meanwhile, adding in fibre loading and bigger fibre size content causes lesser in tensile properties and poor surface interaction between rPP/DBLF composites.

## 1. INTRODUCTION

Nowadays the application of natural fibres in polymer industries looks increasing tremendously [1]. The function of natural fibres as a secondary phase seems enhance the new dimension in structure stability, superior resistance in impact properties, magnificent strength in mechanical properties, superior abrasion resistance as well as thermal stability. In this study, the waste from an injection moulding scrap namely polypropylene (rPP) was loaded with dried banana leaves fibre (DBLF), for rPP/DBLF composites fabrication [1-4]. This green composition between plastic lump and natural fibres have greater and terrific mechanical properties as well as physical properties. Green composition become an outstanding product since it is eco friendly and safe to human application. In this study, dried banana leaves fibre (DBLF) has been applied as functional filler for recycled polypropylene (rPP) matrix which was emitted lump from an injection moulding process. For this intention, the waste polypropylene collected from an injection moulding process, and grounded into fine particles by using an industrial crusher. It follows by, some compounding step and hot compression technique were operated for rPP/DBLF composites production. In principle, natural fibre is commonly used as an extender to reduce the percentage of plastic usage, and increase the mechanical properties. For this reason, to understand the role of DBLF as latest green functional filler for polymer matrix composites, with the specific objectives were to determine the effects of fibre size and fibre loading in rPP composites production

## 2. METHODOLOGY

### 2.1 Raw Materials

The matured banana leaves from *musa acuminata* sp. species taken from reserved area located in IKTBN Sepang and chipped into smaller size at about 40-50mm in length and 1-2mm in width. The chipped leaves dried for conditioning purpose for 24 hours at 80°C. The leaves were grounded to two sieve sizes 10 $\mu$ m and 30 $\mu$ m. the analysis of fibre size was carried out by using Malvern Instruments Mastersizer 2000 version 5.54. The range of measurement area in this system was between 0.020- $\mu$ m to 2000- $\mu$ m. The grounded fibre air conditioned at 80°C and humidity 65% for 3 days before executing fibre size analysis. Recycled Polypropylene (rPP) are collected from the waste produced by injection moulding process. The collected rPP lump was first cleansed and isolated for any contamination or impurities elimination. Lastly the compounding process of rPP/DBLF composites was performed via double steps of melt-blending process at various fibre loadings (0, 10, 20, 30 and 40) wt. %.

### 2.2 Tensile Testing of rPP/DBLF Composites

The tensile test for rPP/DBLF composites were performed in accordance to ASTM D638 – Type 1. The test was carried out at controlled atmosphere of 22 $\pm$ 1°C, at relative humidity of 60%. Testing was performed at 10 mm/mins of cross-head speed by using a Universal Testing Machine (GoTech). For each loading, about five samples were tested for data averaging purpose.

### 2.3 Fracture Surface Morphological Observation of rPP/DBLF Composites

The fracture surfaces of the selected samples of rPP/DBLF composite was observed under the Scanning Electron Microscope (SEM) observation. At first, the fractured surface was mounted onto the stub with carbon tape before being coated with gold-palladium (Au-Pd) thin conductive coating, using a sputter coater model Polaron E-1500, to eliminate the charging effects during observation. The fracture surface images were captured by using Zeiss Evo VPSEM at 7.00kV accelerating voltage for 100x of magnification power at secondary electron detection.



### 3. RESULTS AND DISCUSSION

The following Figure 1 presented both fibre size analysis result of grounded dried banana leaves that has been sieved at two different sizes 10 $\mu$ m and 30 $\mu$ m. Based on Figure 1, multi wide distribution of fibres sizes was recorded, varying from almost 0 to 35 $\mu$ m. The analysis of 10 $\mu$ m size group showed that 18 % of volume recorded

(red line) while the fibre size of 30 $\mu$ m (green line) has peaked at 11% of volume itself. The percentile analysis shows that for both fibre size almost 50 % - 60 % of the screened DBL fibre samples are having sizes in between 10 $\mu$ m - 30 $\mu$ m and the rest of them are out of the range required.

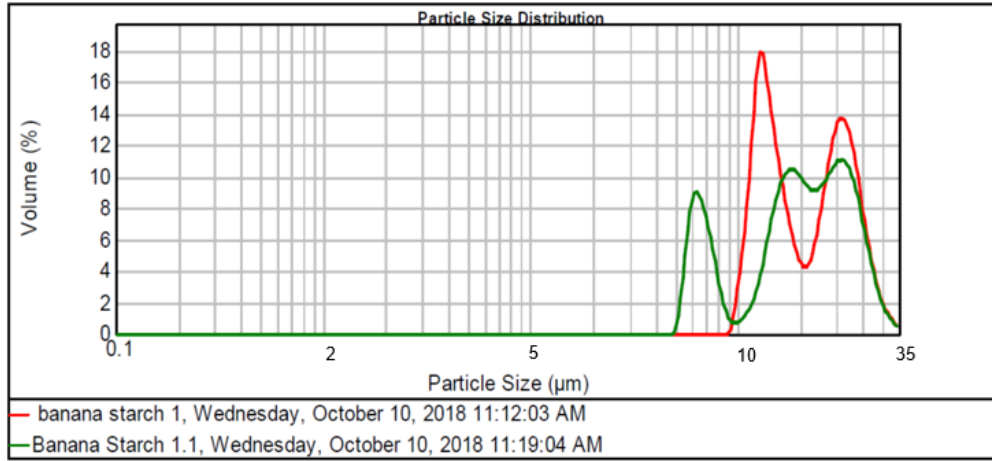


Figure 1 Particle size analysis (PSA) of 10 $\mu$ m grounded DBL fibre (red line) and 30 $\mu$ m DBLF fibre (green line).

Figure 2 shows a scanning electron microscope (SEM) micrograph observation for grounded DBL fibre at 100X of magnification. There a few samples randomly taken, and a mean value was then calculated to yield a final averaged result of 10 $\mu$ m -30 $\mu$ m. Thus, the prepared DBL fibre was verified having the averaged length for both sample sieve sizes about 10.4 $\mu$ m and 32.4 $\mu$ m, these surface and shape feature are important in influencing the matrix-filler interaction, between the rPP and grounded DBL fibre.

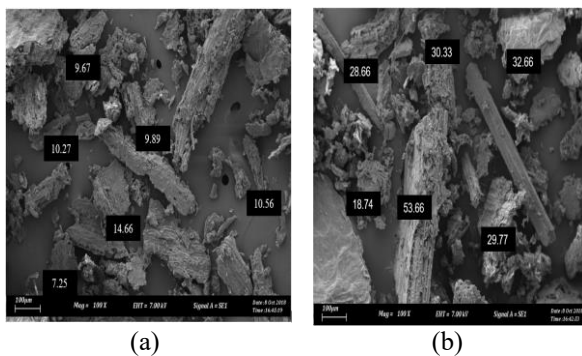


Figure 2 SEM micrograph of raw grounded (a) 10 $\mu$ m and 30 $\mu$ m DBL fibre.

The following Figure 3 has presented the resulted tensile strength (TS) for rPP based composites filled with two different fibre sizes 10 $\mu$ m and 30 $\mu$ m at various loadings (wt.%). It was clearly found that, by DBLF with smaller fibre size into rPP matrix, the TS was significantly increased up to +22.30% of positive improvement (refer to green bar), in comparison to the 30 $\mu$ m DBL fibre size (refer to blue bar). However, adding up of DBLF filler more than 30wt% has reducing the composites performance, which responsible lowering the TS values for both fibre size. Overall results proven that

the size of fibre will play a major role which was produced superior outcome, that make a big impact to the composite properties.

### 4. CONCLUSION

In conclusion, from this study, the effects of DBL fibre loadings as well as the effect of fibre size towards the investigated tensile and fracture morphological properties of rPP/DBLF composites were fully explored and understood. Based on the experimental results, it was found that, about 30wt% of 10 $\mu$ m size DBL fibre addition has enough to enhance the TS for positive improvements compared to 30 $\mu$ m fibre size. This positive finding provides another alternative of degradable plastic-based composite to be selected and utilized for various promising applications.

### REFERENCES

- [1] Ramesh, M., Atreya, T. S. A., Aswin, U. S., Eashwar, H., & Deepa, C. (2014). Processing and mechanical property evaluation of banana fiber reinforced polymer composites. *Procedia Engineering*, 97, 563-572.
- [2] Yin, S., Tuladhar, R., Combe, M., Collister, T., Jacob, M., & Shanks, R. (2013). Mechanical properties of recycled plastic fibres for reinforcing concrete. *Fibre Concrete*, 1-10.
- [3] Bolka, S., Slapnik, J., Rudolf, R., Bobovnik, R., & Mešl, M. (2018). Thermal and mechanical properties of biocomposites based on green PE-HD and hemp fibers. *Contemporary Materials*, 1(8), 80-90.
- [4] Bátori, V., Jabbari, M., Åkesson, D., Lennartsson, P. R., Taherzadeh, M. J., & Zamani, A. (2017). Production of pectin-cellulose biofilms: A new approach for citrus waste recycling. *International Journal of Polymer Science*, 2017, 1-9.



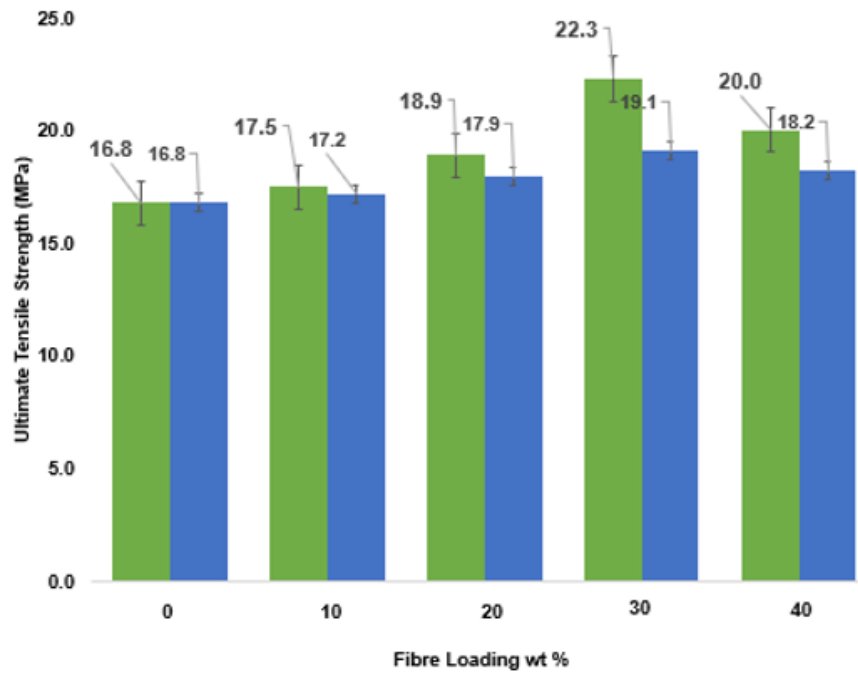


Figure 3 TS plots for fibre size 10µm (green bar) and 30µm (blue bar) DBLF at different wt% of loadings in *rPP* based composites.

# Flexural properties of thermoplastics corn starch reinforced short pineapple leaf fibre composites laminates at various ply

Nazri Huzaimi Zakaria<sup>1,3,\*</sup>, Mohd Zulkifli Selamat<sup>2,3</sup>, Mohd Zamani Ngali<sup>4</sup>, Abd Fuad Ab Ghani<sup>1,3</sup>,  
Nur Rohaiza Izamuddin<sup>1</sup>

<sup>1</sup>) Fakulti Teknologi Kejuruteraan Mekanikal dan Pembuatan, Universiti Teknikal Malaysia Melaka,  
Hang Tuah Jaya, 76100 Durian Tunggal, Melaka, Malaysia

<sup>2</sup>) Fakulti Kejuruteraan Mekanikal, Universiti Teknikal Malaysia Melaka,  
Hang Tuah Jaya, 76100 Durian Tunggal, Melaka, Malaysia

<sup>3</sup>) Centre for Advanced Research on Energy, Universiti Teknikal Malaysia Melaka,  
Hang Tuah Jaya, 76100 Durian Tunggal, Melaka, Malaysia

<sup>4</sup>) Fakulti Kejuruteraan Mekanikal dan Pembuatan, Universiti Tun Hussein Onn Malaysia,  
86400, Parit Raja, Batu Pahat, Johor, Malaysia

\*Corresponding e-mail: nazrihuzaimi@utem.edu.my

**Keywords:** cornstarch; PALF; biopolymer

**ABSTRACT** – This study intends to investigate the characteristic of thermoplastic corn starch (TPCS) composite reinforced short pineapple leaf fibre (PALF) was prepared using laminates (sandwich) methods based on five various plies. The composite was fabricated by using 2mm of fibre length and evaluated the properties of different fibre loading (20 wt%, 30 wt%, 40 wt%, 50 wt% and 60 wt%). The flexural strength and flexural modulus of short PALF/TPCS composite were studied and compared. The PALF content at 50 wt% showed the highest mechanical properties value compared to other fibre content.

## 1. INTRODUCTION

Environmental consciousness, new rules, and legislation are forcing industries to look for new materials that are environmentally friendly [1]. The research community has expressed rising interest in using PALF as to reinforce thermoplastic and thermoset polymer composites due to their excellent mechanical properties compared to other natural fibres [2]. For the development of natural fibre composites, the material construction can easily be manipulated in many ways, such as varying the fibre loadings, fibre ratio, fibre type (short, long), fibre orientation (random, unidirectional, woven), number of ply, and ply stacking sequence [3].

Previous literature review revealed that there are several studies which reported on the effect of ply to the mechanical properties of hybrid natural fibre composite laminates such as for kenaf/Kevlar reinforced epoxy composites [4] and oil palm empty fruit bunch (OPEFB) /jute reinforced epoxy composites [5]. In addition, Mansor et al. [6] also emphasized that the final hybrid composites product quality was also influenced by the ply stacking sequence due to the interaction between the combined fibres and matrix.

In this paper, the biopolymer composite based on natural fibre (PALF) reinforced TPCS composites was prepared by using laminates (sandwich) methods at five various plies. The main objective of this study was to explore the effect of varying fibre loading on the various ply to the PALF reinforced TPCS composite on the flexural properties. Five different ply formations were

developed by using a compression moulding (Hot Press Machine) process. All samples were subjected to flexural tests based on ASTM D790 standard to determine the optimum flexural strength and flexural modulus of the laminates PALF/TPCS composites.

## 2. METHODOLOGY

### 2.1 Raw Materials

Corn starch (CS) used in this study was taken from the manufacturing type and in powder form. CS powder and glycerol were procured from Polyscientific Enterprise Sdn. Bhd. The type of glycerol was Qrec G4018-1-2500. The PALF from Josapine cultivars were purchased from cultivated areas in Kampung Parit Puteri Menangis, Pontian, Johor, Malaysia.

### 2.2 Sample Preparation

Thermoplastics corn starch was prepared from blended 70 wt% of native corn starch and 30 wt% of glycerol via hand-mixed and high speed mixer.

Five various fibre stacking sequences were applied to prepare the laminates PALF/TPCS composites as shown in Table 1 where the total weight of the PALF/TPCS composites was 40g. All short PALF were randomly orientated within the ply.

All laminates were subjected to compression moulding (Hot Press Machine) at 750 kg/cm<sup>2</sup> and at 165 °C temperature for 15 minutes followed by cure for 30 minutes. The laminates were fabricated based on a mild steel mould with fixed length x width x height of 140 mm x 60 mm x 3 mm.

Table 1 Compositions of PALF/TPCS composite laminates (sandwich) at various plies.

Loading	PALF (wt%)		TPCS (wt%)		
20/80	10	10	27	26	27
30/70	15	15	23	24	23
40/60	20	20	20	20	20
50/50	25	25	17	16	17
60/40	30	30	13	14	13

### 2.3 Flexural Testing

Flexural tests were conducted according to ASTM

D-790 at the room temperature. The samples were prepared with dimensions of 140 mm (L) x 13 mm (W) x 3mm (T) by using a circular saw. The tests were carried out on five replications using a Universal Testing Machine (INSTRON 5556) with a 5 kN load cell; the crosshead speed was maintained at 2 mm/min.

### 3. RESULTS AND DISCUSSION

Figure 1 shows the overall results on flexural strength and modulus of PALF/TPCS composite which prepared via laminates method.

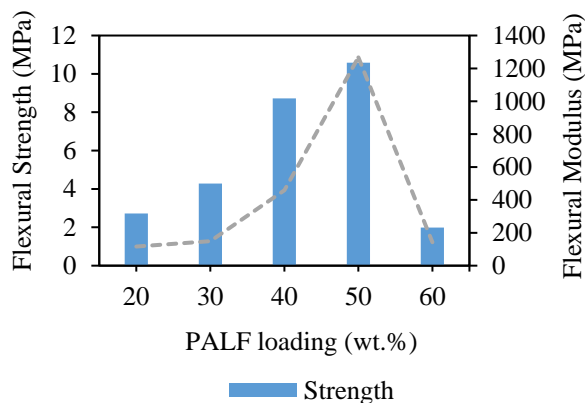


Figure 1 The flexural strength and modulus against PALF loading (wt%).

In general, the flexural test results show increasing trend until the optimum result at 50 wt% and drastically drop at 60 wt% of fibre loading. This trend is similar to the flexural modulus. The highest flexural strength was achieved at 10.58 MPa and flexural modulus was 1266 MPa. Both flexural strength and modulus of PALF/TPCS composites increased with increasing PALF content in the composites. However, the lowest flexural strength was observed at 60 wt% of fibre loading about 1.99 MPa and flexural modulus around 1.42 MPa.

A higher flexural strength of the PALF/TPCS composites might be attributed to a similar hydrophilic character of PALF and TPCS, which led to great compatibility between them. The combination of compatible materials is often associated with improvement in mechanical properties of the resulting materials [7].

### 4. CONCLUSION

Biopolymer composite from TPCS reinforced short PALF was successfully prepared via laminates method in five various ply by using hot press machine in this study. The results show that TPCS and short PALF are compatible. The addition of PALF (up to 50 wt%) able to improve the flexural strength and modulus of composites. PALF reinforced with 50 wt% TPCS shows the highest value of flexural strength and modulus as compared to other composites. Meanwhile, TPCS reinforced with 60 wt% PALF shows the lowest result on flexural properties. Based on this indicator, TPCS blended with 50 wt% PALF has huge potential to be a good biopolymer composites.

### ACKNOWLEDGEMENT

The authors would like to thank Faculty of Mechanical and Manufacturing Engineering, Universiti Tun Hussein Onn Malaysia and Advance Materials Research Group (A-Mat), Faculty of Mechanical and Manufacturing Engineering Technology, Faculty of Mechanical Engineering, Universiti Teknikal Malaysia Melaka for financial sustenance and the utilisation of their facilities and besides the Ministry of Higher Education Malaysia for providing the scholarship award to complete this study.

### REFERENCES

- [1] Juraidi, J. M., Shuhairul, N., Azuan, S. S., & Anuar, N. I. S. (2013). A comparison of tensile properties of polyester composites reinforced with pineapple leaf fiber and pineapple peduncle fiber. In *IOP Conference Series: Materials Science and Engineering* (Vol. 50, No. 1, p. 012071). IOP Publishing.
- [2] Siregar, J. P., Cionita, T., Bachtar, D., & Rejab, M. R. M. (2015). Tensile properties of pineapple leaf fibre reinforced unsaturated polyester composites. In *Applied Mechanics and Materials* (Vol. 695, pp. 159-162). Trans Tech Publications.
- [3] Hamid, N. A., Abdullah, N. H. N., Mansor, M. R., Rosli, M. A. M., & Akop, M. Z. (2010). An Experimental Study of the Influence of Fiber Architecture on the Strength of Polymer Composite Material. *Journal of Mechanical Engineering and Technology (JMET)*, 2(2).
- [4] Yahaya, R., Sapuan, S. M., Jawaid, M., Leman, Z., & Zainudin, E. S. (2015). Effect of layering sequence and chemical treatment on the mechanical properties of woven kenaf-aramid hybrid laminated composites. *Materials & Design*, 67, 173-179.
- [5] Jawaid, M., & Khalil, H. A. (2011). Effect of layering pattern on the dynamic mechanical properties and thermal degradation of oil palm-jute fibers reinforced epoxy hybrid composite. *BioResources*, 6(3), 2309-2322.
- [6] Mansor, M. R., Hadi, M. A. A., Taufiq, M. J., Salim, M. A., & Saad, A. M. (2018). Fabrication of hybrid oil palm empty fruit bunch and kenaf reinforced epoxy composite panels at varying fiber layering sequence. *1st Colloquium Paper: Advanced Materials and Mechanical Engineering Research*, 1.
- [7] The, D. P., Debeaufort, F., Voilley, A., & Luu, D. (2009). Biopolymer interactions affect the functional properties of edible films based on agar, cassava starch and arabinoxylan blends. *Journal of Food Engineering*, 90(4), 548-558.

# Effect of carbon nanotube-silane addition on mechanical properties of chloroprene rubber-filled carbon black

Kok-Tee Lau<sup>1,2,\*</sup>, Jeefferie Abd Razak<sup>2,3</sup>, Hairul Effendy Ab Maulod<sup>1,2</sup>, Noraiham Muhamad<sup>2,3</sup>, Mohamad Hanif Hashim<sup>1</sup>, Solament Arumugam<sup>1</sup>, Hoi Ern Kok<sup>1</sup>, See Ern Chung<sup>1</sup>, Nurzallia Mohd Saad<sup>4</sup>

<sup>1</sup>Fakulti Teknologi Kejuruteraan Mekanikal dan Pembuatan, Universiti Teknikal Malaysia Melaka, 76100 Durian Tunggal, Melaka, Malaysia

<sup>2</sup>Carbon Research Technology Research Group, Advanced Manufacturing Centre, Universiti Teknikal Malaysia Melaka, 76100 Durian Tunggal, Melaka, Malaysia

<sup>3</sup>Fakulti Kejuruteraan Pembuatan, Universiti Teknikal Malaysia Melaka, 76100 Durian Tunggal, Melaka, Malaysia

<sup>4</sup>Sunrich Integrated Sdn. Bhd., 53 & 54, Industrial Estate, 70450 Seremban, Negeri Sembilan, Malaysia

Corresponding e-mail: \*ktlau@utem.edu.my

**Keywords:** Electromagnetic interference (EMI); synthetic rubber; silane coupling agent

**ABSTRACT** – This study is to investigate the effect of carbon nanotube (CNT)-silane addition on tensile strength and elastic modulus of chloroprene rubber (CR)-filled carbon black (CB). The CR-filled CB was prepared by internal mixing, followed by roll-mill process in which CNT-silane dispersion was added. For comparison, CR-filled CB without CNTs and added with as-received CNTs were prepared. CR composite added with CNT-silane dispersion displayed 4% higher tensile strength and elastic modulus than CR-filled CB added with dry CNTs. FESEM micrograph shows CNT-silane dispersion addition produced better CNTs dispersion in the compound, thus verified the mechanical data.

## 1. INTRODUCTION

Recent flexible and stretchable electronics applications create high demands for flexible and durable materials [1]. Chloroprene-filled CNT rubber has been investigated for the electromagnetic shielding application [2]. Nevertheless, there are continuous studies to outcome CNTs agglomeration, for example by Krainoi et al. where CNTs was mixed with rubber in latex form [3]. Although promising results were reported, some of the methods are not feasible and incurs high manufacturing cost. Furthermore, CNT powder becomes airborne quite easily when pouring during compounding process, contributes to materials loss and air contamination. Thus, it is desirable to maintain CNTs in liquid dispersion through improvement in conventional manufacturing processing set up. In this study, we report the effect of CNT-silane dispersion addition on CR-filled CNT on the tensile strength and elastic modulus. Materials and manufacturing process of the compound is also presented.

## 2. METHODOLOGY

CR master batch with formulation as stated in Table 1 was prepared using internal mixer (Yi Tzung) operating at 60 °C, rotor speed of 900 rpm and mixing time of 8 mins. Subsequently, the CR match batch was divided into three smaller portions and then were calendared separately with different formulations (refer Table 2) using two-roll mill (model: MT2-2, Yi Tzung) at rotor speed of 19.3 rpm (front) and 22.5 rpm (back) and mixing

time of 5 min. All chemicals used in the formulations are from industrial grade.

Table 2 shows CNTs was added as second filler for CNT and CNT-Silane samples. During roll-mill, as-received CNTs was added in dry form for CNT samples, whereas, CNTs was added in dispersion form for CNT-Silane samples. CNT-Silane dispersion was prepared with the ultrasonication of 1.25 g Si-69 silane coupling agent in the 100 mL ethanol solution (95%). Then, as-received CNTs was mixed into the Si-69 solution. Additional 100 mL ethanol solution was then added, followed by further agitation by ultrasonication for 60 min. As control, CR compound samples without CNTs (which is an established formulation) were also prepared.

Table1 Formulations of master batch

Chemicals	Loading (phr)
Chloroprene (CR)	100
Zinc oxide (ZnO)	5
Stearic Acid (ST Acid)	0.5
Nocrac AD-F	2
Coumarone Resin (G90)	8
Carbon Black (N550)	40

Sheet samples (sample size = 4) for tensile test were prepared by hot press process in the respective sheet-shaped cavity steel molds, at 160°C and pressure of 110 kg-force for 10 min. Tensile tests were performed according to JIS K 6251 standard using Tensometer (model: UR-2060, U-CAN DYNATEX) to obtain tensile strength and elastic modulus data. Surface of tensile fracture samples were observed using Field-emission Scanning Electron Microscope (FESEM, 3 kV accelerating voltage, secondary electron emission mode, Merlin compact-60-25, Carl Zeis).

## 3. RESULTS AND DISCUSSION

### 3.1 Tensile Test

Tensile strength (TS) with standard error bar plots in Figure 1 show that CNT-Silane addition able to negate the deteriorating effect of CNT addition. TS of samples filled with CNT-Silane is comparable to the controlled samples and was 3% higher than the CNT samples. The low TS of

the CNT samples may be caused by formation of CNTs agglomerations in the CR compound, resulted in an earlier failure. This agglomeration problem was resolved with the usage of CNTs treated with Si-69 coupling agent. Nevertheless, CNT-Silane did not perform well as reinforcement agent, thus the TS did not improve significantly in comparison with controlled samples. It appears that presence of silane provided lubrication effect to the compound which permitted macromolecular chain slippage.

Table 2 Second formulations added during roll mill.

Chemicals	Loading (phr) for		
	CNT	CNT-Silane <sup>#</sup>	Control
Carbon Nanotubes (CNTs)	1	1 <sup>#</sup>	0
Magnesium Oxide (MGO)	4	4	0
Ethylene Thiourea (ETU-80)	0.7	0.7	0.7
N-Cyclohexyl-2-Benzothiazole Sulphenamide (CBS)	0.75	0.75	0.75

<sup>#</sup>Amount of added CNT (in dispersion form) was controlled at 1 phr dry weight of CNTs. Silane and ethanol solution were not included in phr calculation.

However, addition of CNT-silane helped to improve the stiffness characteristic by enhancing the tensile modulus at 300% of elongation (refer Figure 2). This condition might contribute by the ability of silane to assist CNT dispersion during compounding with CR. Better dispersion of CNT-silane provide good network between them within the CR matrix to resist the deformation. This can be the reason of the enhanced stiffness value.

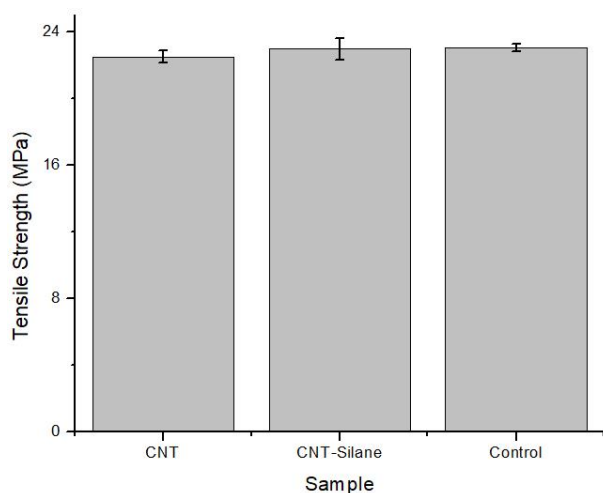


Figure 1 Tensile strength of CR compound samples.

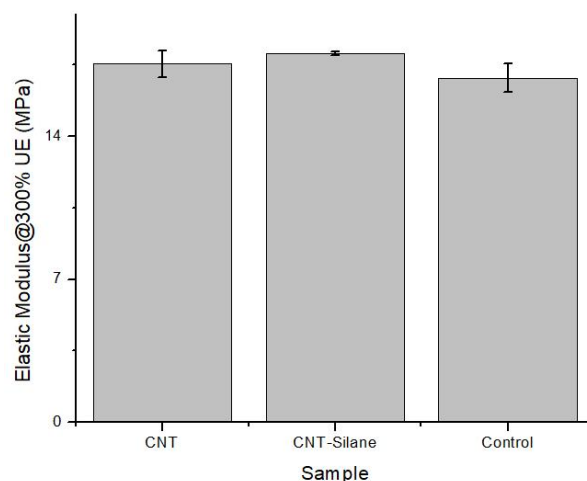


Figure 2 Elastic modulus (at 300% elongation) of CR compound samples.

FESEM micrograph in Figure 3 shows CNTs dispersed better after addition of silane. Thus, verified the mechanical data.

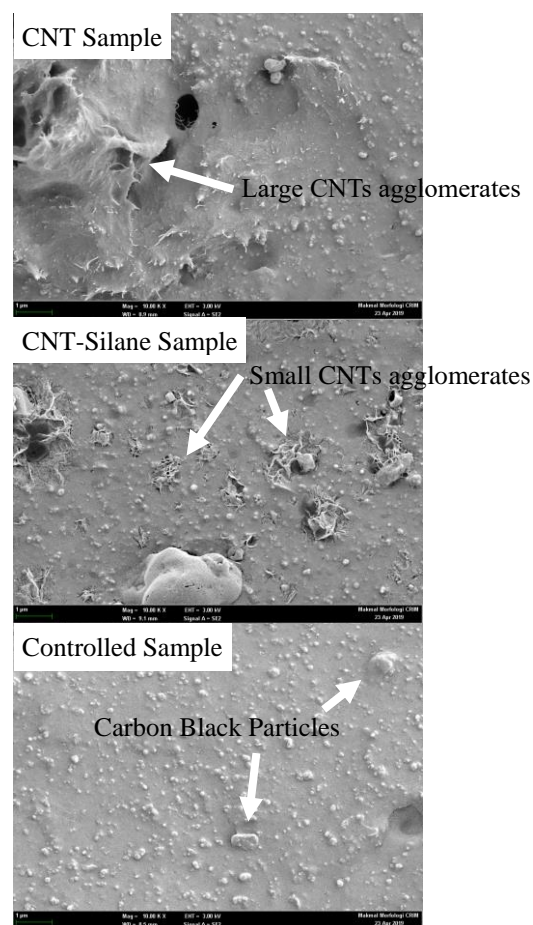


Figure 3 FESEM micrograph of surface of tensile fracture samples.



#### 4. CONCLUSION

CNT-silane addition into CR-filled CB showed higher tensile strength and elastic modulus than CR-filled CB added using as-received CNTs. FESEM showed a better CNTs dispersion in the CR matrix for the former.

Future work needs to investigate the effect of direct mixing of as-received CNTs and silane coupling agent into the CR compound, on the mechanical properties of CR compound. The study could decrease the processing steps of CR compound processing using silane addition.

#### ACKNOWLEDGMENT

The authors wish to thank Sunrich Integrated Sdn. Bhd. for providing sample preparation and mechanical properties characterization facilities.

#### REFERENCES

- [1] Dahiya, R. (2019). E-Skin: From Humanoids to Humans. *Proceedings of the IEEE*, 107(2), 247-252.
- [2] Kapgate, B. P., & Das, C. (2016). Electronic Applications of Chloroprene Rubber and Its Composites. In *Flexible and Stretchable Electronic Composites* (pp. 279-304). Springer, Cham.
- [3] Krainoi, A., Nakaramontri, Y., Wisunthorn, S., Pichaiyut, S., Nakason, C., Kummerlöwe, C., ... & Kiatkamjornwong, S. (2019). Influence of carbon nanotube and ionic liquid on properties of natural rubber nanocomposites. *Express Polymer Letters*, 13(4), 327-348.

# Study of the oil palm empty fruit bunch as fiber reinforcement on composite material

Mohd Fariduddin Mukhtar<sup>1,3,\*</sup>, Mohamed Saiful Firdaus Hussin<sup>1</sup>, Amir Abdullah Muhammad Damanhuri<sup>1</sup>, Khairul Amri Tofrowaih<sup>1</sup>, Khairul Azri Azlan<sup>1</sup>, Noor Saffreena Hamdan<sup>1</sup>, Adam Samsudin<sup>2</sup>

<sup>1</sup>) Fakulti Teknologi Kejuruteraan Mekanikal dan Pembuatan, Universiti Teknikal Malaysia Melaka, Hang Tuah Jaya, 76100 Durian Tunggal, Melaka, Malaysia

<sup>2</sup>) Fakulti Teknologi Kejuruteraan Elektrik dan Elektronik, Universiti Teknikal Malaysia Melaka, Hang Tuah Jaya, 76100 Durian Tunggal, Melaka, Malaysia

<sup>3</sup>) Advanced Manufacturing Centre, Universiti Teknikal Malaysia Melaka, Hang Tuah Jaya, 76100 Durian Tunggal, Melaka, Malaysia

\*Corresponding e-mail: fariduddin@utem.edu.my

**Keywords:** Oil palm; fruit bunch; material

**ABSTRACT** – The aim for this research is to study the characteristics of oil palm empty fruit bunch (OPEFB) as a fiber reinforcement on natural composite. Two group samples used OPEFB with different type of resin which is epoxy and polyester regarding to different fiber volume fraction. Hardness test, impact test and water absorption test were used. Results shows that sample with 50% fiber content displayed the highest hardness and impact value while in water absorption, it also shows the lowest value for both resins. OPEFB behaved as a significant adhesion between the matrix and composite. As a conclusion, to make a better composite, OPEFB and resin matrix should be mixed equally for better characteristics.

## 1. INTRODUCTION

Discovery of new advance material always give ideas for new advance material innovation. Overcome any limitation of the source of material for the traditional composite material such as glass fiber, natural fiber is renewable reinforcement to replace traditional composite material. Natural fiber appears to have low cost and easy to gain as the material is highly renewable and it helps for global sustaining the environment [1].

Nowadays, the replacement of natural fiber in composite polymer is interesting topics as it proves to be good performance from previous study, natural fiber can be an alternative approach because it has many properties and able to increase the strength ratio of the composite [2]. In aim of this research is to study the compatibility of natural fiber with two different resin matrices by using impact test, hardness test and water absorption test.

## 2. METHODOLOGY

OPEFB were used as fiber reinforcement and chopped into smaller size, divided into three part with different fiber volume fraction (25%, 50% and 75%) as in Figure 1 and the fraction were given as in Table 1. The mould prepared size is 20cm x 30cm and waxed with mirror glaze as release agent. The material then fabricated using epoxy and polyester, so there will be two different type of composite panel. Wet hand lay-up is implemented into this fabrication process for both type of resin, as the epoxy resin is for ambient cure. The samples then cut into smaller pieces by following dimension for testing. Total sample prepared for test is six.



Figure 1 Sample of 25% and 50%  $V_f$ .

Table 1 Sample's fiber volume fraction ( $V_f$ ).

Sample	Fiber volume fraction (%)	
	OPEFB fiber	Resin
1	25	75
2	50	50
3	75	25

Samples were then undergone three different test which is hardness test, impact test and water absorption test. For water absorption test, OPEFB composite panel specimens were immersed into distilled water at room temperature for different time duration. Distilled water is used to prevent any additional substance such as chlorine involve in this test to avoid any miss reading result caused by unwanted existence during process. All the specimens are soaked onto different container and for different time duration. The differences between the absorption percentage were calculated using Equation (1).

$$\frac{W_f - W_i}{W_i} \times 100\% \quad (1)$$

Where  $W_f$  = final weight and  $W_i$  = initial weight.

## 3. RESULTS AND DISCUSSION

Figure 2 shows the result of both type of sample with different fiber volume fraction ( $V_f$ ) of Hardness test. The graph shows that sample of OPEFB-polyester is harder than epoxy with the highest percentage 79.2 type D. By referring 75%  $V_f$  while the softest is epoxy with 50%  $V_f$ , 66.6 type D. Roughly, polyester resin is the harder sample based on the graph below.

In Figure 3, for impact test result, the result of the Epoxy-OPEFB shows, the highest result for impact test

is E50 with 50%  $V_f$ , impact amount receive averagely 3.66J compare to other two samples, E75(75%  $V_f$ ), is the lowest with average impact result is 2.20 while E25 (25%  $V_f$ ) is 2.33. The difference value between E75 and E25 is not big.

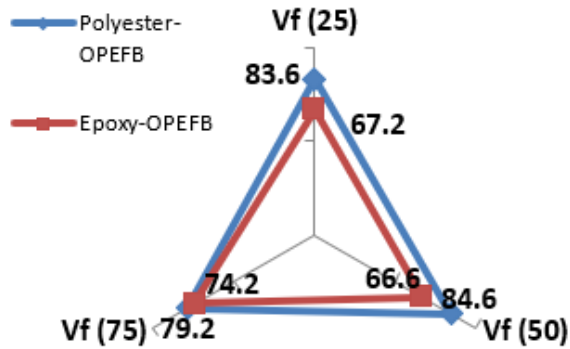


Figure 2 Hardness test.

This result concludes that, the 50%  $V_f$  work well with the matrix resin and performs good impact properties. The highest value from all three polyester-OPEFB impact test is sample P50 with fiber volume fraction is 50%. The lowest value is from sample P25, with average value is only 0.90 Joule, while the average impact value for P75 is 1.16J. From the graph it is indicate the 50%  $V_f$  is holds the highest value of impact.

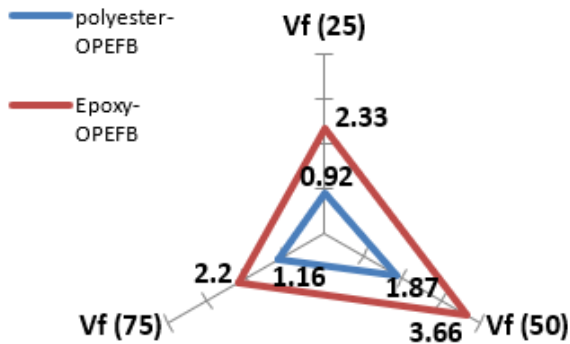


Figure 3 Impact test.

However, the variance of the water absorption for the first 2 days shows all the specimens absorb 1% of water mass then increasingly absorb about 0.845% averagely in next 4 days. The 0.2% different show the absorb activities has slowed down. This is cause by the effect from defects occurs on the specimens. Compare all the three sample, E75 ( $V_f$  is 75%) shows the high absorbed water, while E50 ( $V_f$  is 50%) is the lowest absorbed water then E25 ( $V_f$  is 25%).

Less  $V_f$  should have low absorption rate, this is indicating the fiber is hydrophilic nature that tend to absorb water. At final stage the absorption rate is decrease gradually and the samples having saturated state where there is no area or void to fill in. Each sample's absorption rate ends on 3.2%, 2.4%, 2.931% for E75, E50 and E25 respectively.

While for polyester, With increasingly from 0% of  $V_f$  (the  $W_i$  : initial weight) to 0.6864% absorption for the first two days. The samples (P75) rate increase 0.766% making it total absorption percentage is 1.450%. this rapid rate decreases when final immersion duration ends

on day 10, with total final immersion of P75 is 1.862%. Different with P25 and P50, both of sample absorption result is close different. With the first 48 hours, only 0.475% and 0.526% absorption rate for P25 and P50 respectively.

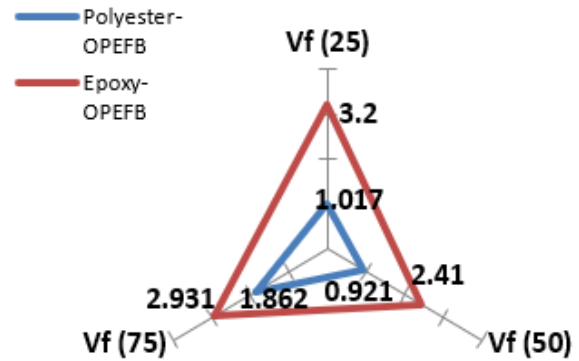


Figure 4 Water absorption comparison.

#### 4. CONCLUSIONS

From the project, all the test has done, and the discussion is explained, so the main objective is successfully achieved. The ability of both type of resin to be compatible with the natural fiber OPEFB have been prove by tests. From the hardness test, it is shows that Polyester-resin is the hardest material compare to Epoxy-OPEFB in this project. This is speculating that the Epoxy resin which using ambient cure maybe have disadvantage.

But, in impact test every specimen work well. The highest impact value is from Epoxy-OPEFB sample, which is indicated, the resin and fiber can work well together with natural fiber performing good impact test result. Other testing is water absorption test. This test is used to calculate the amount rate of water absorption of the sample. The natural fiber is known as hydrophilic material is chosen to study, if the ability to absorb liquid can implement by using two different resins. The result proves that, the higher fiber volume fraction causing the sample to absorb more water, while 50% of  $V_f$  perform better result. From all three tests, the OPEFB can be one of the choices for being reinforced fiber in polymer composite. But, the application of this material is limited to low strength product usage. OPEFB is doubtful to perform well in high strength application.

#### ACKNOWLEDGMENT

The author would like to thank Universiti Teknikal Malaysia Melaka for funding this project through short term grant PJP/2019/FTKEE(3A)/S01655.

#### REFERENCES

- [1] Saheb, D. N., & Jog, J. P. (1999). Natural fiber polymer composites: a review. *Advances in Polymer Technology: Journal of the Polymer Processing Institute*, 18(4), 351-363.
- [2] Al-Oqla, F. M., & Sapuan, S. M. (2014). Natural fiber reinforced polymer composites in industrial applications: feasibility of date palm fibers for sustainable automotive industry. *Journal of Cleaner Production*, 66, 347-354.

# Reduction of corrosion rate of aluminum alloy 6061 through anodization

Md Fahmi Abd Samad\*, Raihana Ramle

Fakulti Kejuruteraan Mekanikal, Universiti Teknikal Malaysia Melaka,  
Hang Tuah Jaya, 76100 Durian Tunggal, Melaka, Malaysia

\*Corresponding e-mail: mdmahmi@utem.edu.my

**Keywords:** Corrosion; aluminum alloy; anodizing

**ABSTRACT** – This paper focuses on reducing the corrosion rate of aluminum alloy 6061 through anodizing. The study involves characterizing corrosion phenomenon in relation to parameters involved in an anodizing process, in particular the current density of anodizing, and its corrosion environment, specifically, the pH value and concentration of sodium chloride (NaCl) solution where the alloy is placed. The cleaning process is in accordance to ASTM G 1-90(1999). It concludes that corrosion rate may be reduced through an increase of current density during anodizing and such improvement was also observed even with high concentration and low pH of corrosion accelerator solution.

## 1. INTRODUCTION

Aluminum alloy has emerged as the best material applied in automotive industries for structural application. It is also known as the second-best material, second only to steel, in metal industry. The preference has been based on characteristics such as light weight, non-rusting properties, reasonably good strength, easy fabrication and favorable economics, coupled with modern metallurgical control of structure and properties.

However, like any other metal material, aluminium alloy suffers from some disadvantages. These include its tendency to serrated yielding during stretching and drawing, loss of strength during annealing of paint bake cycle, and corrosion [1,2].

This paper provides an extension to the study of corrosion protection of aluminium alloy, by relating directly an observed corrosion phenomenon to the parameters of anodizing.

## 2. METHODOLOGY

The raw materials were Aluminum Alloy 6061-T4 sheet. For the anodizing process, the complete list of equipment was as follows:

- a) Beakers
- b) Power supply 0-100 volt
- c) Crocodile clips
- d) Sulfuric Acid ( $H_2SO_4$ )
- e) Test samples (Al-6061)

The material was cut into 30 mm long and 1.695 mm thickness test samples. The samples to be set as the cathode in the anodization was cut as 10 mm width whereas the anode was cut as 30 mm width. Next, each of the samples was placed in designated beaker containing  $H_2SO_4$  and connected to electrical current source where different current density is applied.

After 20 – 30 minutes of anodizing, the samples

were immersed into different concentration of sodium chloride (NaCl) for corrosion acceleration. In accordance to ASTM G 1-90(1999), the cleaning process involves the use of sand paper grade 250 followed by sand paper grade 1250 (as a polishing guide), a solution of 50ml phosphoric acid and 20 g chromium trioxide, and also nitric acid [3].

In the calculation of corrosion rate, the following equation was applied

$$\text{Corrosion rate} = \frac{K \times W}{A \times T \times D}$$

Where:

$K$  – a constant depending on the corrosion unit expression

$T$  – time of exposure in hours

$A$  – area in  $cm^2$

$W$  – mass loss in g

$D$  – density in  $g/cm^3$

The procedure to examine pitting corrosion in this project is referred from ASTM G 46-94 (Reapproved 1999) standard.

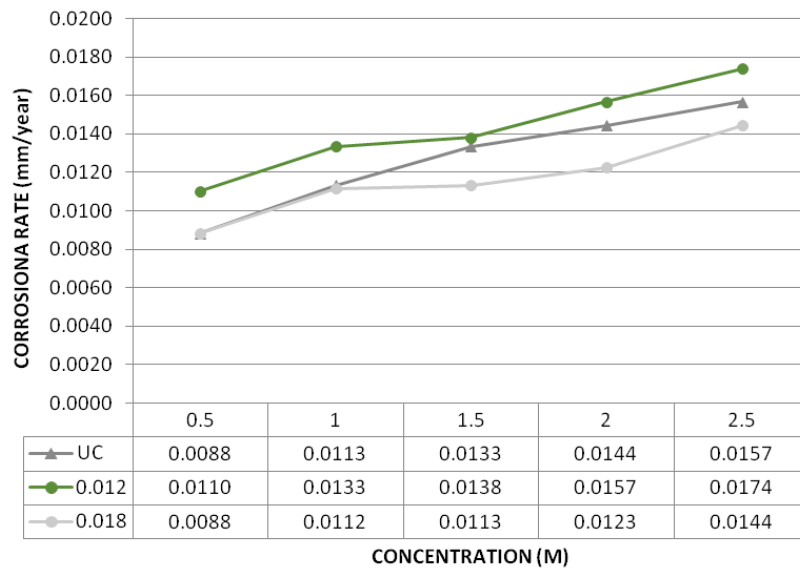
## 3. RESULTS AND DISCUSSION

The rate of corrosion was determined and presented as in Figure 1. It shows that the rate of corrosion increases as the concentration of NaCl increases. From this study, it is also seen that the level of current density also has an effect on the rate of corrosion of the sample. It is obtained that with higher current density, the corrosion rate decreases.

This may be due to high growth rate of oxide when using high current density, as confirmed by Chung et al. [5]. The solution concentration and also the anodizing process characterizes the electrochemical nature of the corrosion process. These factors are of considerable importance when evaluating corrosion resistance.

The plot of the corrosion rate versus pH value of the solution concentration shows that there is a nonlinear descending relationship between the corrosion rate and pH value of the solution (Figure 2). Based on the Pourbaix diagram, within the pH limits of its passive range (generally between 4 to 8.5), aluminum corrodes in aqueous solution because their oxides are soluble in many acids and bases, yielding  $Al^{3+}$  ions in the former and  $AlO_2^-$  ions in the latter [6].

Figure 3 shows two images captured using scanning electron microscope that shows the visual characteristics of the corrosion. It very much resembles pitting corrosion.



Legend: UC: uncoated; 0.012: 0.012 A/mm<sup>2</sup>; 0.018: 0.018 A/mm<sup>2</sup>

Figure 1 Corrosion rate versus concentration of corrosion solution.

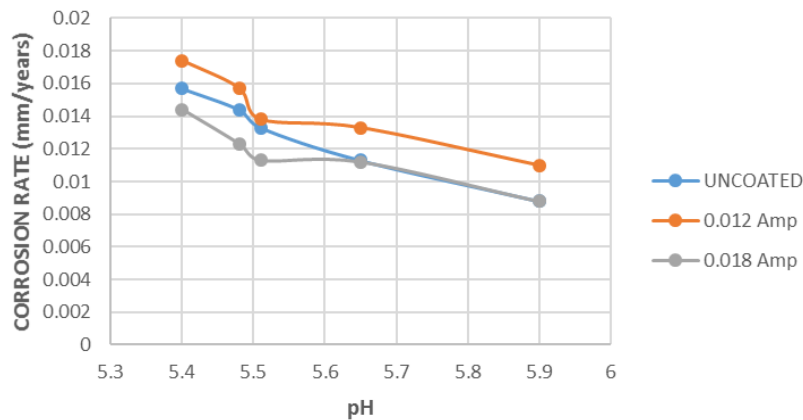
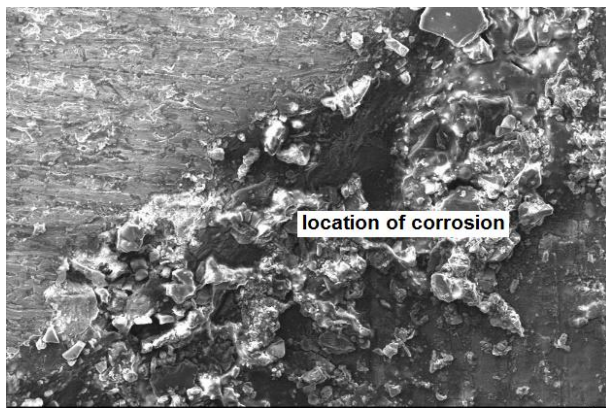
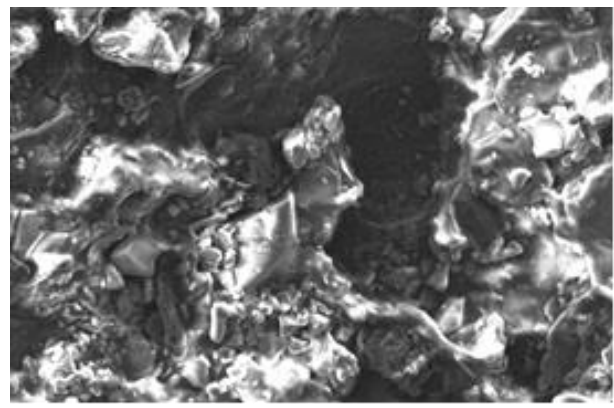


Figure 2 Corrosion Rate versus pH.



(a)



(b)

Figure 3 SEM image for uncoated sample in (a) 1.0 M NaCl solution; (b) 1.5 M NaCl solution.

#### 4. CONCLUSION

The test shows that when in contact with the surface of aluminum alloy 6061, the increase in current density during anodizing decreases the mass loss, hence corrosion rate. Aside from this, this project identified that rate of corrosion in aluminum alloy 6061 has an increasing trend towards the increment of NaCl solution concentration. Furthermore, by the decrement of solution pH value, the rate of corrosion increases. The corrosion

rate may be further reduced with the increase of current density during anodizing.

Other factors that may contribute to rate of corrosion is the electrode potential of material. By referring to the electrode potential, studies have shown that aluminum alloy 6061 is more active than sodium hydroxide (NaOH) and more susceptible to oxidation. A more realistic and practical ranking however may be provided by the galvanic series.



## REFERENCES

- [1] Ghali, E. (2010). *Corrosion resistance of aluminum and magnesium alloys: understanding, performance, and testing* (Vol. 12). John Wiley & Sons.
- [2] Sivasankaran, S. (Ed.). (2017). *Aluminium Alloys: Recent Trends in Processing, Characterization, Mechanical behavior and Applications*. BoD–Books on Demand.
- [3] ASTM Committee G-1 on Corrosion of Metals. (2017). *Standard practice for preparing, cleaning, and evaluating corrosion test specimens*. ASTM international.
- [4] ASTM G46-94. (2005). *Standard guide for examination and evaluation of pitting corrosion*. ASTM international.
- [5] Chung, I. C., Chung, C. K., & Su, Y. K. (2017). Effect of current density and concentration on microstructure and corrosion behavior of 6061 Al alloy in sulfuric acid. *Surface and Coatings Technology*, 313, 299-306.
- [6] Ashby, M. F., & Jones, D. R. H. (2012). *Engineering materials 1: an introduction to properties, applications and design* (Vol. 1). Elsevier.

# Effect of thin metal adhesion layer and thermal annealing process on microheater coil structure quality

Norihan Abdul Hamid<sup>1,3,\*</sup>, Syafeeza Ahmad Radzi<sup>2,3</sup>, Mazree Ibrahim<sup>4</sup>

<sup>1)</sup> Centre for Telecommunication Research Innovation, Universiti Teknikal Malaysia Melaka, Hang Tuah Jaya, 76100 Durian Tunggal, Melaka, Malaysia

<sup>2)</sup> Centre for Robotics and Industrial Automation, Universiti Teknikal Malaysia Melaka, Hang Tuah Jaya, 76100 Durian Tunggal, Melaka, Malaysia

<sup>3)</sup> Fakulti Kejuruteraan Elektronik dan Kejuruteraan Komputer, Universiti Teknikal Malaysia Melaka, Hang Tuah Jaya, 76100 Durian Tunggal, Melaka, Malaysia

<sup>4)</sup> Fakulti Teknologi Kejuruteraan Elektrik dan Elektronik, Universiti Teknikal Malaysia Melaka, Hang Tuah Jaya, 76100 Durian Tunggal, Melaka, Malaysia

\*Corresponding e-mail: norihan.hamid@utem.edu.my

**Keywords:** Micro heater; annealing process; adhesion layer, metal deposition

**ABSTRACT** – Aims of this paper is to investigate and study the effect of metal adhesion layer and thermal annealing process to improve the metal layer quality and bonding of the micro-heating elements so that thermal power generation can be improved. A thin metal adhesion layer is deposited on the borosilicate glass substrate using a metal sputtering process, then the sample was carried out in nitrogen atmosphere by thermal annealing treatment at an optimum of 450°C in 30 minutes. The results show that the quality and the crystal properties of metal has improved besides structural defect and resistance of the conductor was reduced to obtain higher thermal generation.

## 1. INTRODUCTION

The existence of a metallic layer as a heater coil structure for the micro heater on the surface of the borosilicate glass substrate with low resistance value is necessary [1] to enable higher thermal power generation performance. However, a conventional microelectromechanical system (MEMS) fabrication technique has been known to have a high impact on heater elements thus increasing the metal resistance that may lead to the degradation of thermal generation performance.

In general, the adhesion layer may improve the metal adhesion on substrate, reduce resistance and obtain smooth surface [2], while the annealing treatment process may improve crystallinity and energy impurity. No doubt, metal element with lower resistance value will improve the quality of metal conductive layer which has good ohmic contact and reduces the resistance [1, 3].

Therefore, in this study, the effect of the adhesion layer and thermal annealing process on a microheater coil structure were investigated. The influence of annealing treatment on physical metal surface and structure was observed using an optical microscope while SEM is used to analyze the structural properties. Then the performance of heat generation was measured and compared to the previous micro heater coil structure without the adhesion layer and annealing treatment process.

## 2. MICRO HEATER STRUCTURE

The microheater structure consists of microheater built with metal resistive material that has higher thermal conductivity for a heater element structure and deposited on a thin substrate structure made of borosilicate glass material as illustrated in figure 1. For a simple geometry design, ease of fabrication process and produce a higher rate in small volume production, a square meander geometry design of heater element was chosen.

Normally the heater element, induced with the small voltage on the heater pad hence allow current flows through the heater element from one side to another. This conduction process will allow the heater to produce high thermal distribution for various kind of application in microdevice components such as micro pump [4], gas detector [5, 6] and etc. The total dimension of the microheater is approximately 10 mm x 15 mm x 2.4 mm with the thickness material from 1 to 10 um for heater element and substrate respectively. The length of the heater element is approximately 32 mm.

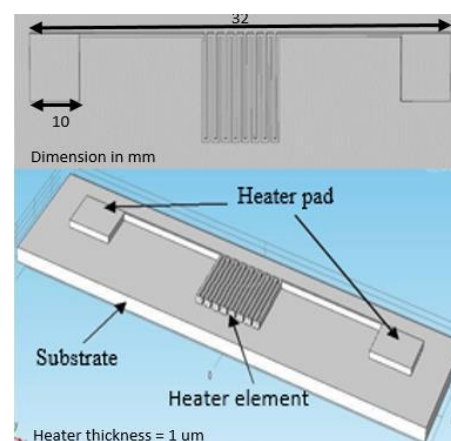


Figure 1 Top and side view of heater structure.

## 3. EXPERIMENTAL PREPARATION

A thin borosilicate glass substrate was cleaned with a common glass substrate cleaning process with acetone, isopropanol and deionized (DI) water. Next, the heater geometry structure was developed using a mask lithography process and immersed into the developer until the pattern appeared on the surface of the glass

substrate. Then, the glass substrate was deposited with or without adhesion layer. In this experiment, 50 nm Chromium (Cr) was chosen as the adhesion layer [2,3,4] due to high binding material strength with oxygen and able to passivate with various many material surfaces [1,3]. Then a higher resistive element of 500 nm Platinum (Pt) was deposited on the top of Cr act as a heater structure element. Both of metal deposition on the glass substrate was done by a metal sputtering process in the sputter chamber with argon ambient at  $2.0 \times 10^{-3}$  Torr, 30 mm working distance and operating current of 30 mA. After that, both metal layers were lifted and immersed in the ultrasonic bath at approximately 2 minutes to reveal the deposited metal heater element structure. The sample then was placed in the furnace for thermal annealing treatment about 30 minutes at a temperature of  $450^{\circ}\text{C}$  to enhance their structural property. The annealing temperature was chosen by considering the effect of the temperature on metal quality previously [1,4, 5]

#### 4. RESULTS AND DISCUSSION

The differences of chromium deposition compared to without any adhesion can be seen clearly at the end of the process using an optical microscope seen in figure 2. The glass substrate with a chromium layer in figure 2 (a) was observed to provide a better adhesive layer, accurate element size, provide a uniform surface and less fracture. While the image in figure 2 (b) shows its bad attachment layer, the element size is smaller than the actual size, uneven surfaces besides there are small fractures and holes on the surface element. In addition, the resistance measurement results also show that elements with a chromium adhesive agent have lower resistance than non-coated metal chromium elements [5].

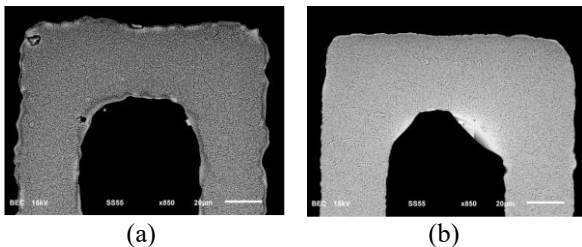


Figure 2 The image of a metal structure with (a) and without (b) Cr as the adhesion layer using an optical microscope.

Figure 3 depicted surface morphology of thin metal structure layer before and after the annealing process using scanning electron microscopy (SEM) machine. Figure 3(a) shows that the metal structure is slightly uniform with the substrate cover with some void and cracks. From the surface topology, it can be seen that there is a different size of cluster composed on the metal microparticle, while Figure 3(b) shows an improvement in crystallinity after the annealing process. Hence the surface enhanced with smaller voids, pinholes or cracks on the substrate. At the same time, the annealing treatment also gives an improvement in mean grain size. This may be due to the tendency of a particle to shake and made coalesce arrangement from smaller clusters into larger clusters during the annealing process [3].

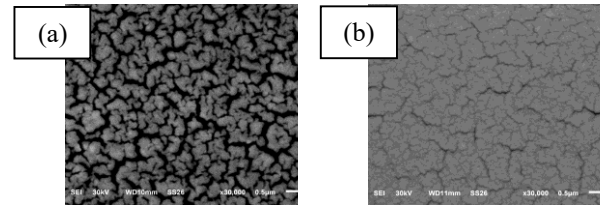


Figure 3 SEM image of platinum (a) before (b) after annealing.

#### 5. CONCLUSION

Effect of thin metal adhesion and thermal annealing process on micro heater coil structure quality have been investigated and studies. No doubt by depositing an adhesion layer on the borosilicate glass surface its can give better attachment of metal structure hence, provide an actual size and uniform surface of the heater element structure. At the same time, better adhesion can also reduce the conductor element. While thermal annealing treatment on metal conductor structure can reduce the structural defect and conductor resistance thus improve the crystallinity. By reducing the resistance, lower power consumption will be achievable to obtain higher thermal generation.

#### ACKNOWLEDGMENT

Authors are thanks to Centre for Telecommunication Research Innovation (CeTRI), Fakulti Kejuruteraan Elektronik and Kejuruteraan Komputer, Universiti Teknikal Malaysia Melaka for the moral, operational and financial support they provided

#### REFERENCES

- [1] Yunas, J., Said, M. M., Pawinanto, R. E., & Majlis, B. Y. (2016). Enhancement of metal coil quality on selective p-silicon based planar electromagnetic coil by thermal annealing process. *Microsystem Technologies*, 22(10), 2493-2497.
- [2] Chang, W. Y., & Hsihe, Y. S. (2016). Multilayer microheater based on glass substrate using MEMS technology. *Microelectronic Engineering*, 149, 25-30.
- [3] Abdul Hamid, N., Yunas, J., Yeop Majlis, B., Hamzah, A. A., & Bais, B. (2015). Microfabrication of Si3N4-polyimide membrane for thermo-pneumatic actuator. *Microelectronics International*, 32(1), 18-24.
- [4] Butt, M. A., & Fomchenkov, S. A. (2017). Thermal effect on the optical and morphological properties of TiO<sub>2</sub> thin films obtained by annealing a Ti metal layer. *Journal of the Korean Physical Society*, 70(2), 169-172.
- [5] Hamid, N. A., Majlis, B. Y., Yunas, J., & Dehzangi, A. (2013, September). Annealing effects on structural and electrical properties of micro heater conductor element. In *RSM 2013 IEEE Regional Symposium on Micro and Nanoelectronics* (pp. 77-80).
- [6] Bedoui, S., Gomri, S., Samet, H., & Kachouri, A. (2016, March). Design and electro-thermal analysis of a platinum micro heater for gas sensors. In *2016 13th International Multi-Conference on Systems, Signals & Devices (SSD)* (pp. 558-561).

# Characteristics of the superficial oxide layer on the aluminium (99.4% purity) granules during in-situ melting

Aslinda Saleh<sup>1,\*</sup>, Mohd Hasbullah Idris<sup>2</sup>, Norfazillah Talib<sup>3</sup>, Haslina Abdullah<sup>3</sup>, Lee Woon Kiow<sup>3</sup>

<sup>1)</sup> Faculty of Engineering Technology, Universiti Tun Hussien Onn Malaysia,  
Pagoh Higher Education Hub, 84600 Pagoh, Muar, Johor, Malaysia

<sup>2)</sup> School of Mechanical Engineering, Faculty of Engineering, Universiti Teknologi Malaysia,  
81310 UTM Skudai, Johor, Malaysia

<sup>3)</sup> Faculty of Mechanical and Manufacturing Engineering, Universiti Tun Hussein Onn Malaysia,  
86400 Parit Raja, Batu Pahat, Johor, Malaysia

\*Corresponding e-mail: aslinda@uthm.edu.my

**Keywords:** In-situ melting; aluminum; oxidation

**ABSTRACT** – This study was conducted to develop alternative approach for a pouring free casting process that would reduce the turbulence due to pouring action in the conventional casting process resulted with porosity in the cast product. The in-situ melting was employed for investment casting of 99.4% purity aluminium (Al) granules by heating the granules at the temperature 700, 750, 800 and 850°C for 30 and 60 min. However, the Al granules oxidised forming superficial ( $\text{Al}_2\text{O}_3$ ) layer that increased in thickness as the temperature and duration were increased hinders the complete melting of the granules.

## 1. INTRODUCTION

Casting is a versatile manufacturing process which can cast any metal into products such as household products and even engineering parts. However producing sound aluminium (Al) casting is challenging due to the nature of the liquid aluminium that absorbed hydrogen from the environment which resulted with gas porosity in the solidified casting. In fact, the reaction of liquid aluminium alloy with moisture and/or oxygen develops very thin oxide layer on the surface of the molten metal when pouring into mould the entrained and folded surface oxide ( $\text{Al}_2\text{O}_3$ ) film known as the bifilm developed due to turbulence. The bifilm remains in the solidified casting act as nucleation sites for the pore/porosity formation that decrease the mechanical properties of the casting [1].

Several attempts have been employed to reduce the porosity such as by melt treatment, and adopt turbulence free filling system. The melt treatment requires molten metal degassing with inert gas [2], degassing with ultrasonic vibration [3,4], fluxing with chloride and fluoride salt [5].

Alternatively, turbulence free filling system including tilt casting [6], bottom filling [7], low pressure bottom filling [8], in-situ melting [9] and in-situ microwave casting [10] were developed to overcome the issue. It was found that the in-situ melting and in-situ casting approaches has potential to become a pouring free casting process however the former design of experiment and equipment used in in-situ casting was complex and costly. The in-situ melting approach is more simple and economic however melting granular metal or alloy is a challenge to the metal caster as they oxidised during

heating at high temperature which hindered the complete melting of the granules. This study investigates the characteristics of the superficial oxide layer formed on the pure aluminium granules that effects the incomplete melting of those granules.

## 2. METHODOLOGY

50g of the 99.4 % pure aluminium (Al) granules with cylindrical shape sized 4mm diameter and 5-6mm height were charged into a pre-prepared cylinder ceramic investment casting mould made of six layers of ceramic with measured mould thickness between 6 to 7mm. The filled mould were shaken gently by hand to allow the granules occupy the entire mould geometry. The mould was placed in a high temperature muffle furnace (KSL-1800X for heating at four different temperatures of 700, 750, 800 and 850°C for the duration of 30 and 60 min. The furnace accuracy and the heating rate was  $\pm 1^\circ\text{C}$  and  $10^\circ\text{C}/\text{min}$  respectively. The heated samples were left to cool slowly in the furnace.

Metallography samples were prepared and characterised using the field emission scanning electron microscopy (FESEM) equipped with energy dispersive x-ray spectroscopy (EDS).

## 3. RESULTS AND DISCUSSION

It was visually observed that the pure Al granules unable to completely melted and produced a casting even after being heated at the temperature 850°C which is beyond its melting temperature (660°C). However the heated Al granules were agglomerated took the shape of the ceramic investment casting mould which indicated the granules might partially melted or fully melted however being encapsulated by superficial oxide layer as previously described by the author [11].

### 3.1 Morphology of the superficial oxide layer

SEM observation revealed the morphology of the Al granules after heated at the temperature of 850°C for 30min containing oxides particles as shown in Figure 1. The oxide particles presence as individual oxide nodules at the certain area while some oxides were agglomerated. The oxides formed on the surface of Al granules heated at 700 and 750°C individually dispersed while for 800°C the individual oxides grew line by line and agglomerated on the surface. The growth of the oxide nodules was due

to the migration of ions simultaneously occurred either by diffusion of Al to the oxide-gas interface or the oxygen ion transported to the oxide-metal interface through the cracks on the oxide layer [12].

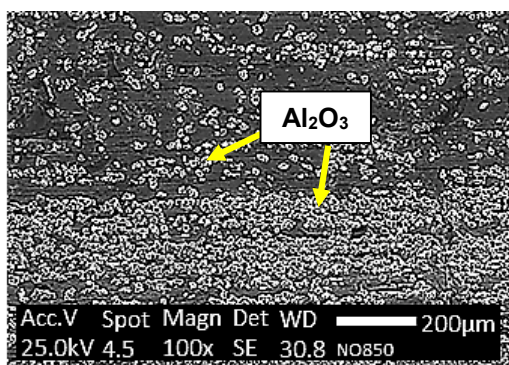


Figure 1 Oxide particles on the Al granule after heated the temperature of 850°C for 30min.

### 3.2 Oxide element and thickness

Figure 2 shows the EDS peaks indicated the presence of 68.79 wt % Al and 31.21 wt % O in the sample which proved that the Al granules oxidized during in-situ melting forming a superficial oxide layer which is the aluminium oxide ( $\text{Al}_2\text{O}_3$ ).

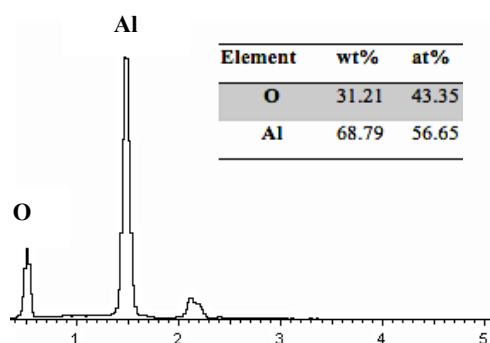


Figure 2 EDS analysis result of the Al granules after heated the temperature of 850°C for 30min.

While, Table 1 listed the thickness of the superficial oxide layer (measured from the cross section cut sample) were increased when the Al granules were heated at the temperature of 700, 750, 800 and 850°C for both heating duration of 30 and 60 min. In average, prolonged heating duration from 30 to 60 min increased the thickness of the oxide layer. It was due to the cracking of the oxide layer at elevated temperature (850°C) facilitating the Al ion diffusion to the oxide surface and oxidised as it in contact with air resulted with the increased oxide size [13].

Table 1 Thickness of the superficial oxide layer.

Temp. (°C)	Duration (min)	
	30	60
	Thickness (µm)	
700	0.949	0.704
750	0.286	0.588
800	1.109	1.988
850	8.515	10.610

## 4. CONCLUSION

It can be concluded that the superficial oxide layer on the surface of the heated Al granules is aluminium oxide ( $\text{Al}_2\text{O}_3$ ) that randomly presence as individual nodules on the granules' surface (700 and 750°C), line up (800°C) and uniformly agglomerated (850°C). Prolong heating duration and elevated temperature (850°C) had greater influence on the increment of the superficial oxide layer thickness. The increased of oxide layer thickness as the temperature was increased hindered the possibility of the in-situ melting of the Al granules eventhough was heated beyond the melting temperature due to the tiny melted Al was encapsulate by the oxide.

## REFERENCES

- [1] Dispinar, D., & Campbell, J. (2011). Porosity, hydrogen and bifilm content in Al alloy castings. *Materials Science and Engineering: A*, 528(10–11), 3860–3865
- [2] Dispinar, D., Akhtar, S., Nordmark, A., Di Sabatino, M., & Arnberg, L. (2010). Degassing, hydrogen and porosity phenomena in A356. *Materials Science and Engineering: A*, 527(16–17), 3719–3725
- [3] Barbosa, J., & Puga, H. (2017). Ultrasonic melt processing in the low pressure investment casting of Al alloys. *Journal of Materials Processing Technology*, 244, 150–156
- [4] Haghayeghi, R., Bahai, H., & Kapranos, P. (2012). Effect of ultrasonic argon degassing on dissolved hydrogen in aluminium alloy. *Materials Letters*, 82, 230–232
- [5] Puga, H., Barbosa, J., Azevedo, T., Ribeiro, S., & Alves, J. L. (2016). Low pressure sand casting of ultrasonically degassed Al7SiMg alloy: Modelling and experimental validation of mould filling. *Materials & Design*, 94, 384–391.
- [6] Harding, R. A., Wickins, M., Wang, H., Djambazov, G., & Pericleous, K. A. (2011). Development of a turbulence-free casting technique for titanium aluminides. *Intermetallics*, 19(6), 805–813.
- [7] Wang, T., Yao, S., & Shen, W. (2015). A submerged-gate casting method. *Journal of Materials Processing Technology*, 222, 21–26.
- [8] Jafari, H., Idris, M. H., Ourdjini, A., & Kadir, M. R. A. (2013). Influence of flux on melting characteristics and surface quality of in-situ melting AZ91D. *Materials and Manufacturing Processes*, 28(2), 148–153.
- [9] Saleh, A., & Idris, M. H., (2015). Oxidation of pure aluminium granules during in-situ melting. *Advance Materials Research*, 1125, 28–32
- [10] Anžel, I. (2000). High temperature oxidation of metals and alloys. *Metallurgija-Journal of Metallurgy*, 325–336.
- [11] Coker, E. N. (2013). The oxidation of aluminum at high temperature studied by Thermogravimetric Analysis and Differential Scanning Calorimetry. *Sandia National Laboratories*, 7–9.



# Thrust force and tool wear investigation of micro drilling for carbon fiber reinforced polymer (CFRP) material

N. Syuhada Nasir<sup>1,\*</sup>, N. Ab Wahab<sup>1</sup>, R. Izamshah<sup>2</sup>, H. Sasahara<sup>3</sup>, S.A. Sundi<sup>1</sup>

<sup>1)</sup> Fakulti Teknologi Kejuruteraan Mekanikal dan Pembuatan, Universiti Teknikal Malaysia Melaka, Hang Tuah Jaya, 76100 Durian Tunggal, Melaka, Malaysia

<sup>2)</sup> Advanced Manufacturing Center, Universiti Teknikal Malaysia Melaka, Hang Tuah Jaya, 76100 Durian Tunggal, Melaka, Malaysia

<sup>3)</sup> Department of Mechanical Systems Engineering, Tokyo University of Agriculture and Technology, Japan

\*Corresponding e-mail: nsyuhada\_mn@yahoo.com

**Keywords:** CFRP; thrust force; tool wear

**ABSTRACT** – Micro drilling of Carbon fiber reinforced polymer (CFRP) poses numerous challenges due to its anisotropic structure and non-uniform material properties. High cutting force and rapid tool wear are few of the common problems in dealing with this material which correlate with the drilling parameters. Therefore, understanding on the relationship between the parameters and the materials response is crucial for the success of the drilling process. Experimental micro drilling process with variable spindle speed and constant feed was carried out to investigate the effects of machining parameter on thrust force and tool wear. It was observed that, thrust force and tool wear have small effect towards the parameter range studies. Hence, it can be concluded that the investigation work need to be extends by taking into accounts on the influence of feed rate and range of parameter study.

## 1. INTRODUCTION

CFRP is widely use especially for aircraft and automotive component. It provides high strength to weight ratio and excellence material properties [1]. In general, CFRP components are produced near to net shape which required additional machining process especially for the assembly process [2]. Drilling CFRP poses numerous challenges due to its anisotropic structure and inhomogeneity of material properties between the plies [3]. Therefore, selection of optimum parameter plays important role to achieve good hole quality at low cost and shorter cycle time [4].

Challenge in drilling the CFRP can be divided into two different categories which are on the tool and the material itself [5]. Defects on the CFRP like delamination and fiber pullout are commonly occur during drilling process [6]. This paper will emphasize on the tool wear and thrust force. Few studies revealed that the delamination rate are related to thrust force and it can be noted that minimum damage can be obtained by controlling the thrust force below the critical value which significantly related with the cutting parameters namely spindle speed and feed rate [7-10].

## 2. METHODOLOGY

### 2.1 Experimental Setup

The experiments were based on micro drilling CFRP composites panel at different spindle speed and constant feed rate. The micro drilling process was carried

out using router machine Haas Gantry Router with the maximum spindle speed of 10,000 rpm. The cutting parameters were used in this experiment is tabulated in Table 1.

The holding fixture which ensured the safety gap between panel and dynamometer was fabricated and used throughout the experiments. The fixture was mounted on a 3-axis Kistler 5233A1 dynamometer for measuring drilling thrust force. Experiment setup is shown in Figure 1.

Table 1 Cutting parameters.

Parameter/Levels	1	2	3
Spindle speed (rpm)	10,000	9,000	8,000
Feed rate (mm/min)	200	200	200
No. of drilled hole	400	400	400

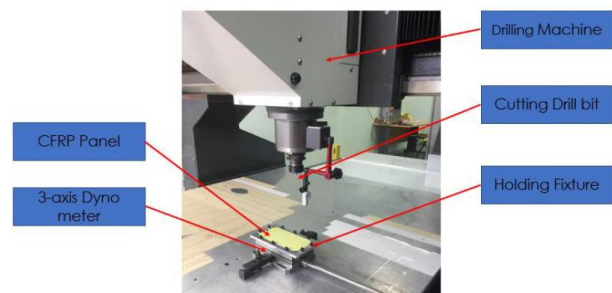


Figure 1 Experimental setup.

### 2.2 Workpiece and Cutting Tools

CFRP composites panels with dimension of 184 mm x 86 mm and maximum thickness of 3.8 mm were used as the workpieces. The panels were manufactured by Hexcel© based on AS4 Carbon Fiber and epoxy matrix with 57.42% nominal fiber volume [11].

Two (2) flutes TiAlN coated solid carbide drill bit with diameter of 0.9 mm and tolerance of +0.004 mm was used. The drill bit has point angle of 130°. Recommended from supplier, minimum spindle speed is 8000 rpm and maximum cutting depth is 9.2 mm [12]. A new fresh drill bit was employed for all the experimental runs.

### 2.3 Experiment's Responses

During the experiments, the thrust force values was measured using 3-axis Kistler 5233A1 dynamometer and

the output from dynamometer was processed by DynoWare software. After the experiments, each tool was observed and captured by using Scanning Electron Microscope (SEM) with 80 times magnification.

### 3. RESULTS AND DISCUSSION

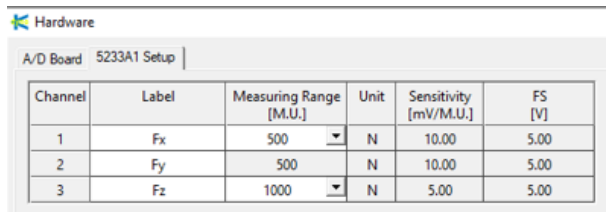
#### 3.1 Experimental Result of Thrust Force

Table 2 shows the result of thrust force for all the experiments. From the table, the average thrust force for all trial were almost similar which were in the range 3.6 N. There are two possible reasons for this reason, firstly is due to the range of applied spindle were too small that result in small thrust magnitudes and secondly due to the thickness of the material that are too thin which produced less impact [13].

Table 2 Thrust force.

Exp.	F <sub>x</sub>	F <sub>y</sub>	F <sub>z</sub>	Average Thrust Force (N)
1	1.740	1.800	3.662	<b>3.662</b>
2	1.755	1.862	3.623	<b>3.632</b>
3	1.785	1.846	3.662	<b>3.662</b>

However, since the values were almost similar for all the experiments, the setting of the dynamometer have re-confirmed. We found that the range of force was set on the control unit was not match with the setting in DynoWare software. Both setting should have similar range as per Figure 2 for F<sub>x</sub>, F<sub>y</sub> and F<sub>z</sub>. This error might cause the values of average force that we obtained become inaccurate.



Channel	Label	Measuring Range [M.U.]	Unit	Sensitivity [mV/M.U.]	FS [V]
1	F <sub>x</sub>	500	N	10.00	5.00
2	F <sub>y</sub>	500	N	10.00	5.00
3	F <sub>z</sub>	1000	N	5.00	5.00

Figure 2 DynoWare interface for range of force.

#### 3.1 Experimental Result of Tool Wear

Image of tool wear was observed under SEM after the experiment. Figure 3 shows the comparison of drill bit before and after each of the experiment. From Figure 3, it can be observed the degradation of the cutting edge material after 400 of holes. In addition, the cutting-edge roundness (CER) diameter increase progressively with the number of drilled compare for all of the experimental runs. It indicated that the cutting edge progressively affected by adhesion wear due to the abrasiveness of the chips produced from the CFRP material [14].

However, accurate estimation of tool life can't be predicted since the tool orientation placed under the SEM need to be properly marked on the same location before and after the drilling process. As for future investigation, special purpose jig needs to be fabricated prior to experiment to ensure the tool orientation and angle are standardizing for accurate measurement.

### 5. CONCLUSION

In conclusions, it was found that the spindle speed has less significant impact on the thrust force. However, for future experimental work the spindle speed range can be further increase. Also, feed rate variation and its interaction with the spindle speed towards thrust force and tool wear are subject that worth to be studied.

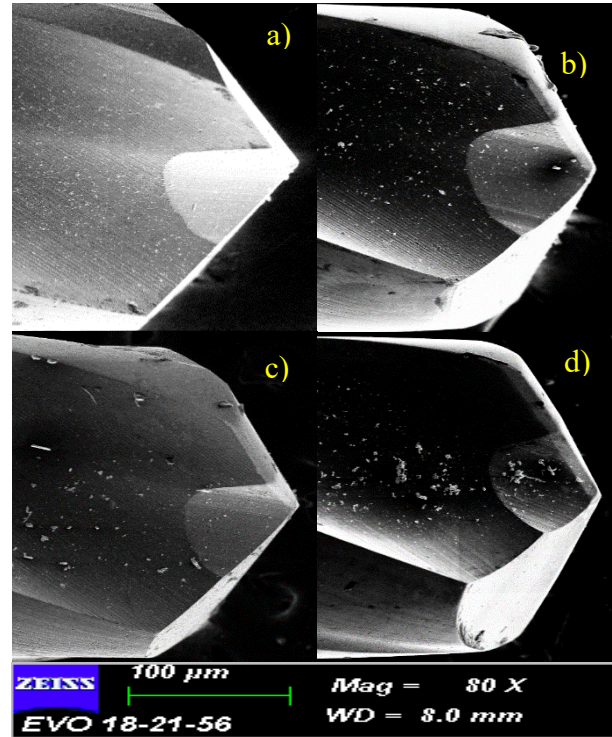


Figure 3 SEM tool image under (a) new tool, (b) Exp. 1, (c) Exp. 2 and (d) Exp. 3.

### ACKNOWLEDGEMENT

This work is partially supported by Universiti Teknikal Malaysia Melaka (UTeM) and the Malaysia Ministry of Higher Education for the financial funding under Grant No. FRGS/2018/FTKMP-AMC/F00387.

### REFERENCES

- [1] Jaafar, M. F., Salleh, M. S., Izamshah, R. Hassan, M. H., Sundi, S. A., Hafiz, M. S. A., & Kasim, M. S. (2019). Influence on thrust force and delamination for one shot drilling of carbon fibre reinforced plastic. *International Journal of Mechanical & Mechatronics Engineering*, 19(1), 43–56, 2019.
- [2] Voss, R., Henerichs, M., & Kuster, F. (2016). Comparison of conventional drilling and orbital drilling in machining carbon fibre reinforced plastics (CFRP). *CIRP Annals*, 65(1), 137-140.
- [3] Sauer, K., Dix, M., & Putz, M. (2018). Process Forces Analysis and a New Feed Control Strategy for Drilling of Unidirectional Carbon Fiber Reinforced Plastics (UD-CFRP). *Journal of Manufacturing and Materials Processing*, 2(3), 46.
- [4] Shunmugesh, K., & Pannierselvam, K. (2016). Optimization of Process Parameters in Micro-drilling of Carbon Fiber Reinforced Polymer (CFRP) Using Taguchi and Grey Relational

- Analysis. *Polymers and Polymer Composites*, 24(7), 499-506.
- [5] Faraz, A., Biermann, D., & Weinert, K. (2009). Cutting edge rounding: An innovative tool wear criterion in drilling CFRP composite laminates. *International Journal of Machine Tools and Manufacture*, 49(15), 1185-1196.
- [6] Su, F., Zheng, L., Sun, F., Wang, Z., Deng, Z., & Qiu, X. (2018). Novel drill bit based on the step-control scheme for reducing the CFRP delamination. *Journal of Materials Processing Technology*, 262, 157-167.
- [7] Tsao, C. C., & Chiu, Y. C. (2011). Evaluation of drilling parameters on thrust force in drilling carbon fiber reinforced plastic (CFRP) composite laminates using compound core-special drills. *International Journal of Machine Tools and Manufacture*, 51(9), 740-744.
- [8] Tsao, C. C., & Hocheng, H. (2003). The effect of chisel length and associated pilot hole on delamination when drilling composite materials. *International Journal of Machine Tools and Manufacture*, 43(11), 1087-1092.
- [9] Ho-Cheng, H., & Dharan, C. K. H. (1990). Delamination during drilling in composite laminates. *Journal of Engineering for Industry*, 112(3), 236-239.
- [10] Alhadeff, L. L., Marshall, M. B., Curtis, D. T., & Slatter, T. (2019). Protocol for tool wear measurement in micro-milling. *Wear*, 420, 54-67.
- [11] Hexcel Composites, S. A. (2010). HexPly® M21 product data sheet, publication FTA002e.
- [12] Hoffmann Group. (2018). Data Sheet for Solid carbide HPC micro-drill +0.004 0,9 mm.
- [13] Joshi, S., Rawat, K., & Balan, A. S. S. (2018). A novel approach to predict the delamination factor for dry and cryogenic drilling of CFRP. *Journal of Materials Processing Technology*, 262, 521-531.
- [14] Hassan, M. H., Abdullah J., Mahmud, A. S., & Supran, A. (2018). Effect of drill geometry and drilling parameters on the formation of adhesion layer in drilling compositemetal stack- up material. *Journal of Mechanical Engineering, SI 5*(2), 90-98.

# Thermal properties and structure morphology of SLSG/SBE: Effect of filler content

Zurina Shamsudin<sup>1,\*</sup>, Masturah Mesri<sup>1</sup>, Rafidah Hasan<sup>2</sup>, Jariah Mohamad Juoi<sup>1</sup>, Zaleha Mustafa<sup>1</sup>

<sup>1)</sup> Fakulti Kejuruteraan Pembuatan Universiti Teknikal Malaysia Melaka, Hang Tuah Jaya, 76100 Durian Tunggal, Melaka, Malaysia

<sup>2)</sup> Fakulti Kejuruteraan Mekanikal, Universiti Teknikal Malaysia Melaka, Hang Tuah Jaya, 76100 Durian Tunggal, Melaka, Malaysia

\*Corresponding e-mail: zurina.shamsudin@utem.edu.my

**Keywords:** Soda lime silicate glass; spent bleach earth; eggshell

**ABSTRACT** – The influence of different filler content on the properties of recycle glass composite was investigated. Samples prepared involved direct sintering process. This study is focused on thermal properties using thermogravimetric analysis (TGA) and microstructural analysis by using scanning electron microscopy (SEM). The results showed that high loading of filler content reduced percentage of weight loss of the samples. Microstructure analysis indicated that the present of pores in recycle glass composites was contributed by less amount of filler content.

## 1. INTRODUCTION

Waste materials from soda lime silicate glass (SLSG) and spent bleach earth (SBE) in the environment have high potential to become a critical factor to human, animals and vegetation when concentration of waste in excess [1]. Recycling is the best way to reduce waste disposal and convert into beneficial product [2]. Generally, waste glass has turned into glass-ceramic composite via conventional method which is heat treatment that involve two stages which are nucleation and crystallization [3]. Salleh et al (2018) worked on SLSG reinforced with SBE reported that crystallization without nucleation stage has shown improvement on densification which enhanced properties glass-ceramic composite [3]. However, the densification has a limit which depends on the percentage of base composition and the thermal properties. These properties played a role in controlling the final properties of the glass composite. In this study, natural waste from eggshell (ES) is introduced as filler in SLSG/SBE composite which similar with cockle shell that contains about 94wt% calcium carbonate ( $\text{CaCO}_3$ ) in its composition and has applied as filler in waste glass [4,5]. The use of ES in waste glass has not much been reported in literature. Thus, with estimated thermal properties and microstructure data, it is expected to identify some factors that lead to the development of SLSG/SBE/ ES composite. Structural morphology will be examined in order to relate the properties of composite with the effect of ES inclusion.

## 2. METHODOLOGY

Glass waste from soda lime silicate glass (SLSG) was collected from the household waste. The preparation of the glass waste undergoes crushing, planetary ball mill and sieving at 100 $\mu\text{m}$  and 40 $\mu\text{m}$ . ES were collected from

household kitchen and then crushed using planetary ball mill and sieve to fine powders (<40  $\mu\text{m}$ ). The raw SBE has undergone a cleaning process to extract oil using sonication process followed by filtration and dry in drying oven until the SBE was in powdery form. Particle size of SLSG, SBE and ES was determined using particle size analyzer, Mastersizer 2000 (Malvern Instrument Ltd model). The compositions shown in Table 1. All samples were produced using conventional ball milling and uniaxial pressing before sintering. The green bodies were proceeded to sintering treatments using laboratory electric furnace Carbolite 1300 model at 800°C at constant heating rate of 2°C /min and 1 hour holding time. Thermal properties were conducted using thermogravimetric analysis (TGA) (TA instrument Q50). Three types of raw materials weighed at 15mg and placed on aluminum pan then heated to 1000°C at 10°C /min. The microstructure of the glass waste composites observed using SEM EVO 50 at accelerated 15kV. Surfaces of the specimen were coated with a conductive platinum layer using Mini Sputter Coater (UK).

Table 1 Ratio of filler content in recycle glass composite

Sample code	SLSG (wt %)	SBE (wt %)	ES (wt %)
A	65	32	3
B	60	34	6
C	55	36	10

## 3. RESULTS AND DISCUSSION

TGA curve for SLSG, SBE and ES is presented in Figure 1. Upon heating the SLSG, SBE and ES powders to 1000°C at 10°C /min, the sample showed endothermic and exothermic peaks which represented as transition glass,  $T_g$ .  $T_g$  is the center of temperature range in which a noncrystalline solid changes from glass brittle to viscous. The value of glass transition was determined by referring derivatives weight curve.

The intersection between two points that showed endothermic slope represented  $T_g$ . The  $T_g$  of SLSG was determined approximately 514.27°C [3] while SBE is 680°C and ES is 432.48°C. Percentage of weight loss at  $T_g$  for SLSG is as much 0.0008613 mg (0.006485%), for SBE is 0.5184 mg (3.934%) and ES is 2.819 mg (20%). The weight loss indicates quantity in mass of the material burned at degradation temperature. The loss in weight is due to pyrolysis of the material upon the nature of the in



situ degradation reaction of the samples. Figure 1 shows SBE contributed high percentage of weight loss compared to SLSG and ES. TGA curve shows that the residue is where the powders fully heated from 0°C until 1000°C has detected. Weight of SLSG that fully heated is 13.25 mg (99.73%), SBE is 9.125mg (69.25%) and ES is 10.39 mg (73.69%).

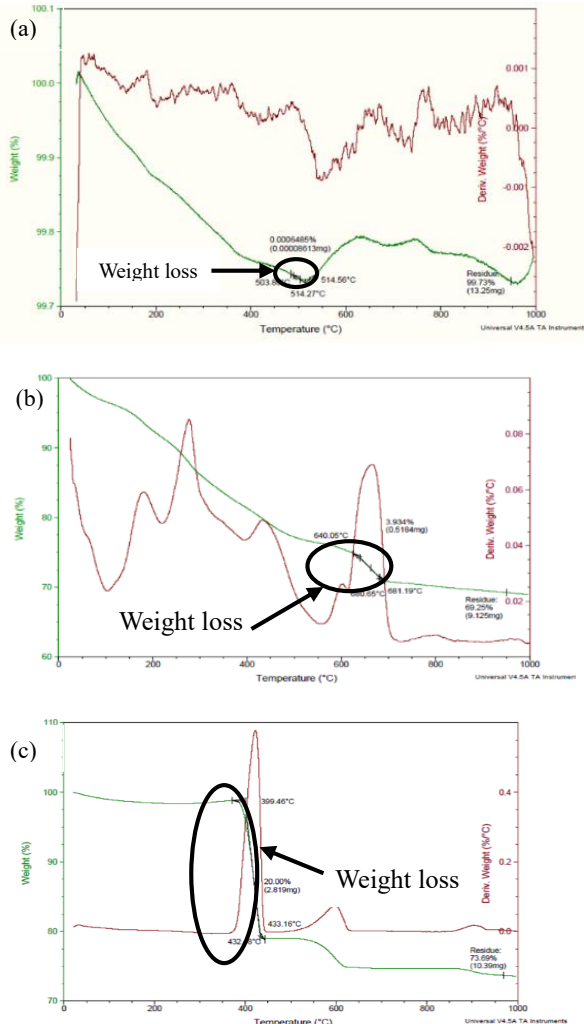


Figure 1 TGA curve for (a) SLSG, (b) SBE, (c) ES.

The TGA results with the microstructure observed in Figure 2. Generally, the increased in weight percent ratio of ES will reduce pores denoted in circular since ES is dominant and less degrade within the composite. As shown in Figure 2 (c), ES with 10wt% produces less pore as filler content increase and presumed to strengthen the microstructure by becoming dense and adhere to SLSG. Compared to 3wt% of ES sample, more closed pores were observed which may be attributed to imperfections in composite.

#### 4. CONCLUSION

Results in this study illustrate the amount of filler content effect to the thermal properties and microstructure of the materials. Recycle glass ceramic

has been sintered at 800°C at rate of 2°C/min and 1 hour holding time. The increased of filler content decreased the percentage of weight loss. SEM analysis showed the variation of microstructure because of the changes in filler content. Therefore, less filler content produced pores appeared to be closer and denser which reveal the filler content influence the composite.

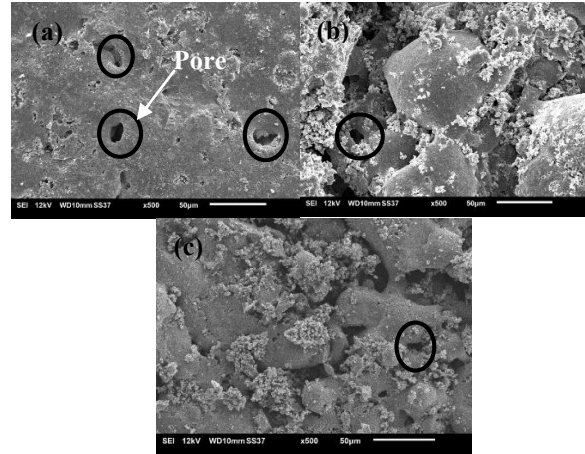


Figure 2 SEM analyses for (a) 3wt%, (b) 6wt%, (c) 10wt%.

#### ACKNOWLEDGEMENT

The authors would like to thank the financial support from Universiti Teknikal Malaysia Melaka through Grant FRGS/2018/FKP-AMC/F00380.

#### REFERENCES

- [1] Mohamed, M., Yusup, S., & Maitra, S. (2012). Decomposition study of calcium carbonate in cockle shell. *Journal of Engineering Science and Technology*, 7(1), 1-10.
- [2] Jia, S., Chen, K., & Chen, Z. (2018, February). Research on the Properties of the Waste Glass Concrete Composite Foundation. In *IOP Conference Series: Earth and Environmental Science* (Vol. 113, No. 1, p. 012098). IOP Publishing.
- [3] Salleh, N., Shamsudin, Z., & Mustafa, J. J. Z. (2017). Effects of heating rates and SBE loading on sintered properties of spent bleach earth/recycled glass composite. *Journal of Mechanical Engineering and Sciences*, 11(4), 3104-3115.
- [4] Souza, M. T., Maia, B. G., Teixeira, L. B., de Oliveira, K. G., Teixeira, A. H., & de Oliveira, A. P. N. (2017). Glass foams produced from glass bottles and eggshell wastes. *Process Safety and Environmental Protection*, 111, 60-64.
- [5] Shamsudin, Z., Razali, A. H., Suzaim, F. H., Mustafa, Z., Rahim, T. A., & Hodzic, A. (2018). Preliminary investigation on the physical properties and morphological of sintered cockle shell/recycled soda lime silicate composite. *Journal of Advanced Manufacturing Technology*, 12(1 (3)), 125-138.



# Design optimization of a new material for portable magnetic clamping plate for conventional milling process

N. Ab Wahab\*, Syafiq Abdul Latiff, Tuan Nur Anis Anisha Tuan NuneK, Hambali Boejang, N. Syuhada Nasir

Fakulti Teknologi Kejuruteraan Mekanikal dan Pembuatan, Universiti Teknikal Malaysia Melaka,  
Hang Tuah Jaya, 76100 Durian Tunggal, Melaka, Malaysia

\*Corresponding e-mail: norfariza@utem.edu.my

**Keywords:** Stainless steel 304; milling process; spindle speed

**ABSTRACT** – This research was carried out to study Design Optimization of a New Material for Portable Magnetic Clamping Plate for Conventional Milling Process. The purpose of this project to replace the type of plate material used on the MagCLAMP product from PVC to stainless steel 304. The three parameters are spindle speed, feed rate and time setting. Taguchi method is used in the experiment. This experiment failed because the MagCLAMP product was unable to function properly. However, analytics data for the time setting parameter has been recorded. This project has its own limit to hold some thin and small magnetic materials.

## 1. INTRODUCTION

The milling machine is the flexible conventional machine tools with extensive metal cutting capabilities. Milling includes various types of operations and machines, based on the scale from small individual parts to large and heavy grinding operations. Moreover, the importance of studying the clamping system in milling operations is evident when the time distribution in milling is studied: According to Sandvik Cormorant, up to 20% of the time is devoted to loading or unloading and setting of the pieces on the clamping system, an identical percentage that occupies the actual machining time [1].

In addition, today's machines have the capability to machine up to five axes, but most conventional clamping do not give access to all five faces of a part. These magnetic clamps usually use electromagnets or permanent magnets to hold materials or workpieces during machining [2].



Figure 1 Portable magnetic clamping (MagCLAMP).

## 2. METHODOLOGY

The method is used to achieve the objective of the project that will accomplish a perfect result. Design optimization of portable magnetic clamping includes problem statement, material selection, improvement design for portable magnetic plate, comparisons between existing plate and optimization plate, and quotation of optimization plate.

The selection of plate material was carried out after doing some research. The type of material used as a plate for the MagCLAMP product is stainless steel 304. Stainless steel 304 is an austenitic steel type having at least 18% chromium and 8% nickel is combined with a carbon maximum of 0.08% [3].

Table 1 Physical properties of stainless steel 304.

Type of material	Percentage
Chromium	18%
Nickel	8%
carbon	0.08% Max

Table 2 The comparison between existing and optimization of the MagCLAMP plate.

Contains	Existing	Optimization
Material	PVC plate	Stainless steel 304
Cost	Cheaper	Less cheap
Durability	Required to change	Long lasting
Mass	Minimize the mass	Maximize the mass to product
Machining process	Water jet	Laser cut

Table 3 Bill of material of plate (BOM).

No .	Part Name	Expectation size (mm)	Types of material	Price	Data
1	MagCLAMP plate	(200 x 200 x 2) mm	Stainless steel 304	60.00	1

In laser cutting, the raw material stainless steel 304 must be cut in the diameter 154 mm. Flatness test had been carried out to inspect the change or variation on the part's surface. Soft material has a better rigidity of the flexible clamping compared to hard material such as aluminium [4]. Before laser cutting, machining process is run, the programming about the drawing of plate needs to be complete in the main computer system. The thickness of the stainless steel 304 is 2 mm. Figure 2 shows the dimension of PVC plate produce from the

machining of water jet.

The machining parameters used are Depth of cut (DC), Spindle speed (N), and Feed rate (f). The effect of machining parameters on surface roughness is evaluated and the optimum cutting condition for minimizing the surface roughness is determined. The predicted values are confirmed by using validation experiments. A L9 orthogonal array, Taguchi method and analysis of variance (ANOVA) are used to formulate the experimental layout, to predict the optimal choice for Portable Mag Clamp by analyzing the effect of each parameter for milling machining characteristics.

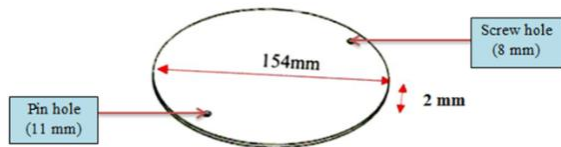


Figure 2 The dimension of PVC plate.

### 3. RESULTS AND DISCUSSION

Through machining parameter testing, all information can be discussed whether the expected results will meet the stated objectives or there are any problems that cause the study cannot be continued as expected. As a result, the facing process as shown in figure 3 to be carried out on the specimen cannot be continued as the specimen moves when it is subjected to a cutting tool milling machine.



Figure 3 Facing process on the mild steel specimen.

Different ways have been done to restore magnetic force, but the all things did not give a good result, until the idea of converting the original plate type had been done. However, the conversion to the PVC plate does not imply that the magnetic force is strong again. Specimens are still moving when applied cutting tools with lower spindle speed 410 rpm. Further experiments to obtain sample specimen machining cannot be carried out. In other words, the objective of the project to obtain data analysis using the Taguchi method is failed.

On averages the value of conventional vice milling shown in Figure 12 is 55.0 Sec, while the value for portable magnetic clamping is 7.9 Sec. The difference the

installation of portable magnetic clamping on the milling machine was more efficient and faster than the existing clamping. Apart from fast installation, the ability to use it to handle machining work can be done quickly

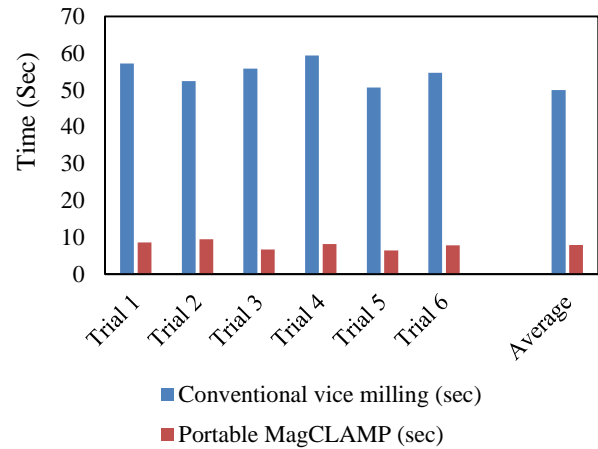


Figure 4 Comparison chart between two types of clamps.

### 4. CONCLUSION

In conclusion, this plate change was successfully implemented and achieved the first objective of the thesis. However, the study to obtain the analysis data through the Taguchi method was unsuccessful. This is due to the problem with the portable magnetic clamping product itself. The portable MagCLAMP product is unable to function properly due to its weak magnetic attraction. The specimens used in the study move from their original state when machining process was carried out. Other than that, the study to compare the speed of installation of two clamping, conventional vice milling, and portable magnetic clamping was successfully performed. The result of time setting parameter was tabulated in the table.

### REFERENCES

- [1] Cantano, J., Alonso, J. M., Peláez, G., Gago, I., Ulloa, A. F., & Ares, J. E. (2015). Magnetic chuck failure prediction: towards the use of non-conventional clamping in milling operations. *Procedia engineering*, 132, 419-426.
- [2] Felix, A., & Melkote, S. N. (1999). Effect of workpiece flatness and surface finish on the holding force of a magnetic chuck. *Journal of manufacturing science and engineering*, 121(4), 811-814.
- [3] Michler, T. (2016). Austenitic Stainless Steels. Reference Module in Materials Science and Materials Engineering. doi:10.1016/b978-0-12-803581-8.02509-1
- [4] Ab Wahab, N., Rani, M. H. B. A., bin Nordin, A. K., bin Nordin, N. F., bin Ibrahim, M. A., Basar, M. F., & Boejang, H. B. (2018). Design and Development of Fixable Clamping for Milling Machine Based on Machining Performance. *International Journal of Applied Engineering Research*, 13(1), 576-581.